Institute of Paper Science and Technology
Atlanta, Georgia

IPST Technical Paper Series Number 634

Mathematical Modelling of the Flotation Deinking Process

F. Bloom and T.J. Heindel

January 1997

Submitted to
Mathematical and Computer Modelling

INSTITUTE OF PAPER SCIENCE AND TECHNOLOGY
PURPOSE AND MISSIONS

The Institute of Paper Science and Technology is a unique organization whose charitable, educational, and scientific purpose evolves from the singular relationship between the Institute and the pulp and paper industry which has existed since 1929. The purpose of the Institute is fulfilled through three missions, which are:

- to provide high quality students with a multidisciplinary graduate educational experience which is of the highest standard of excellence recognized by the national academic community and which enables them to perform to their maximum potential in a society with a technological base; and
- to sustain an international position of leadership in dynamic scientific research which is participated in by both students and faculty and which is focused on areas of significance to the pulp and paper industry; and
- to contribute to the economic and technical well-being of the nation through innovative educational, informational, and technical services.

ACCREDITATION

The Institute of Paper Science and Technology is accredited by the Commission on Colleges of the Southern Association of Colleges and Schools to award the Master of Science and Doctor of Philosophy degrees.

NOTICE AND DISCLAIMER

The Institute of Paper Science and Technology (IPST) has provided a high standard of professional service and has put forth its best efforts within the time and funds available for this project. The information and conclusions are advisory and are intended only for internal use by any company who may receive this report. Each company must decide for itself the best approach to solving any problems it may have and how, or whether, this reported information should be considered in its approach.

IPST does not recommend particular products, procedures, materials, or service. These are included only in the interest of completeness within a laboratory context and budgetary constraint. Actual products, procedures, materials, and services used may differ and are peculiar to the operations of each company.

In no event shall IPST or its employees and agents have any obligation or liability for damages including, but not limited to, consequential damages arising out of or in connection with any company's use of or inability to use the reported information. IPST provides no warranty or guaranty of results.

Mathematical Modelling of the Flotation Deinking Process

by

Frederick Bloom
Department of Mathematical Sciences
Northern Illinois University
DeKalb, IL 60015

and

Theodore J. Heindel
Engineering and Paper Materials Division
Institute of Paper Science and Technology
Atlanta, GA 30318

Abstract

The overall flotation deinking process can be divided into four basic microprocesses: (1) collision or capture of an (ink) particle by an air bubble, (2) adhesion of an (ink) particle to the air bubble by sliding, (3) development of a three-phase contact at the air bubble/water/particle interface, and (4) bubble/particle stability or instability after an aggregate is formed; each of these microprocesses have an associated probability that they will occur successfully in a flotation cell.

In this paper, the associated probabilities of each microprocess are employed in the development of a kinetic-or population balance-type model of the overall flotation process. The overall model contains two kinetic contants: The first, k_1, governs the overall probability of a free ink particle successfully intercepting and adhering to an air bubble; the second, k_2, is a measure of the probability that a bubble/particle aggregate pair will become unstable and split to yield a "new" free ink particle.

The solution to the kinetic model is presented in terms of k_1 and k_2, which are themselves functions of system parameters such as bubble and particle physical properties (e.g., diameter, density), fluid properties (e.g., viscosity, surface tension), etc. From this solution, a definition of a theoretical flotation efficiency, as well as other system performance parameters, are presented.

Key words: flotation deinking, population balance model, microprocess probabilities, bubble/particle interaction, process efficiency

Contents

I Introduction: The Basic Sequence of Events in Flotation Deinking.

Flotation deinking is a separation process which employs swarms of air bubbles to separate ink particles from a wastepaper pulp suspension. The flotation technique itself has been widely used for more than a century in the mineral processing industry. During the past 30 to 50 years, the flotation process has been adapted to the pulp and paper industry for the separation of ink particles, toner particles, and other undesirable particles from cellulose fibers during the recycling of wastepaper products. As pointed out by, e.g., Paulsen et al. [1] "although considerable progress has been made in applying flotation to paper recycling, many significant questions remain, including: (1) details of the phenomenological nature of the process and the fundamental mechanisms which underlie it; (2) the ways in which the hydrodynamics, the physico-chemical nature, and the operating parameters of the system interact; and (3) theoretical and model descriptions of the overall process."

In the flotation process, swarms of small bubbles rise through agitated liquid tanks with suspended pulp and contaminant particles. The bubbles preferentially attach to naturally or chemically hydrophobized contaminant particles, carrying them to a froth layer at the surface of the agitated tank where they are removed. Flotation cells were originally designed for mineral flotation and these cells were used to separate ink particles from wastepaper in the 1950s (McCool [2], Ferguson, [3]). Since then, flotation cells have been specifically designed for flotation deinking with cell designs varying with respect to their geometry, operating parameters, and flow configurations; despite the many design differences, however, they all operate on similar principles, and in all modern flotation systems three separate processes take place in tandem: (1) aeration, whereby air bubbles are introduced into the grey pulp; (2) mixing, where bubbles and stock are intimately mixed to maximize bubble/particle

interation; and (3) separation, where bubbles and bubble/particle aggregates are allowed to separate from the bulk mixture and are skimmed away.

In this paper, we focus our efforts on the theoretical modelling of the overall flotation deinking process. Early efforts at modelling flotation processes focused on the mineral processing industry; the survey paper of Woodburn [4] is a good source for such work, while more recent efforts are discussed in the monograph of Schulze [5] who noted that the basic aim of physically describing the essential microprocesses in the overall flotation process was to enable one to construct a flotation model that would permit "the major aspects of the flotation process to be described by a set of differential equations." One consistent theme in the modelling of flotation has been to treat the overall process as a multistage probability process; such an approach is directly tied to the idea of treating the overall flotation mechanism as a sequence of microprocesses. As indicated in Pan et al. [6], the sequence of microprocesses in flotation deinking is based on the "relative hydrophilic and hydrophobic tendencies of finely divided solid phases (the ink particles) towards water and air bubbles." Flotation chemicals (surfactants) are added to the pulp mixture in a flotation cell so that the surface of the ink particles becomes hydrophobic which, in turn, helps the ink particles attach to the air bubbles that are injected into the cell to aerate the pulp mixture. As for the sequence of microprocesses themselves, these can generally be ordered as follows: (a) the approach of a particle to an air bubble with the subsequent collision with, or interception of, the particle by the bubble (for particles the size of a typical ink particle, the main focus here is on the zone of possible interaction which is created when the particle approaches to within a sufficiently small distance of the bubble); (b) the formation of a three-phase contact angle after sliding of the particle along the thin liquid film which separates the particle from the bubble and subsequent thinning and rupture of this film; and (c) the stabilization of the

bubble/particle aggregate and its transport to the froth layer for removal.

Early work on modelling the overall flotation process includes the work of Gaudin [7], Schuhmann [8], and, especially, Sutherland [9]. As recently as 1992, Pan et al. [6] have written that how the overall flotation deinking process events are "controlled hydrodynamically, how they depend on operating parameters or variables such as bubble size and bubble size distribution or temperature, and how they are influenced by the chemical nature of the system are all questions of considerable interest but which can not be answered from a theoretical standpoint at the present time. Models are needed to combine these (elementary) process parameters to help understand the mechanisms of flotation."

Schulze [5] credits Bilsing [10] with being among the first to try to combine, in a kinetic- or population growth-type model, the concept of a hierarchival process structure with the probabilities of the individual elementary processes by using a kinetic equation of the form $\frac{dc}{dt} = kc$, where c would represent the concentration of free particles in a flotation cell and the rate constant k would depend on the number of bubble/particle 'collisions' per unit time (in a control volume of the cell) as well as on the probabilities associated with the individual flotation processes. The model which we elaborate on in this paper follows the pattern of the basic strategy delineated above, but is more in accord with the formulation of logistic population growth models as opposed to the simple exponential-type population growth (or kinetic) model described above. Even more elaborate (partial differential equation) transport balance models, which involve not only time variations in particle concentrations due to bubble/particle aggregate formation and destruction, but also account for convection and diffusion processes, have been hinted at by Schulze [5] and, more recently, by Plate and Schulze [11].

We now elaborate further on the elementary processes that occur in flotation deinking;

detailed mathematical models for each of the individual processes described below will be sketched in §II. To begin with (Fig. 1), we note that for bubble/particle collisions with respect to particles of the size considered in this report, interception of a particle by a bubble can only take place if the trajectory of the particle is within a streaming tube of radius R_c, the so-called capture radius. As we will specify in §II, the interception probability is then given by $(R_c/R_B)^2$, and the determination of an expression for R_c then depends on whether one models the flow in the flotation cell around a particular bubble as a Stokes flow, a potential flow, or a flow intermediate to these.

Insert Fig. 1.

With particles the size of prototypical ink particles removed by flotation ($\sim 20-200\ \mu m$), attachment of a particle to a bubble by means of an impact collision appears to be an insignificant event. Thus, in our formulation of the problem, we will not speak of the probability of collision but only of the probability of capture or interception of a particle by a bubble. On the other hand, unlike, e.g., Pan et al. [12], we will not refer to the process of attachment of an ink particle to a bubble by virtue of the particle sliding over the film surrounding the bubble as a 'collision' process; rather we will, like Schulze [13-15] refer to this as an adhesion process and label, in §II, the probability associated with it as P_{asl} for "probability of adhesion by sliding." It turns out that adhesion by sliding will usually occur not only when the inertia of the particle is relatively insignificant but when the bubble is (said to be) completely rigid, i.e., completely covered with surfactant through absorption.

During the process of sliding of the particle along the surface of the thin (liquid) film, which separates the particle from the bubble, the film (usually referred to as the 'disjoining' film), with an initial thickness of h_0 may thin down to a critical thickness at which point rupture of the film occurs with the then (possible) subsequent development of the three-

phase contact between the particle, liquid film, and bubble (Fig. 2). When the particle slides over the surface of the disjoining film around a bubble a certain minimal time, the so-called induction time, τ_i, is required for the disjoining film to thin to the point where film rupture can occur. Thus, if τ_{sl} represents the sliding time, then $\tau_{sl} \geq \tau_i$ must hold, and, moreover, (Fig. 1) adhesion by sliding must occur for the touching angle ϕ_T in the range $0 < \phi_T \leq \frac{\pi}{2}$.

Insert Fig. 2

If an ink particle successfully adheres to a bubble, then the next microprocess of concern is the stability or instability of the bubble/particle aggregate against the stresses experienced during elevation into the froth layer; this process is governed by the ratio of the adhesive forces F_{ad} between the particle and the bubble to the detaching forces F_{det} and leads to the specification of a probability P_{stab}, which will be delineated in §II. The determination of the forces F_{det} depends in a critical fashion on how one models the acceleration generated in the (usually) turbulent flow field in the flotation cell. As noted by Schulze [5], most mineral flotation cells have been designed in such a fashion as to produce "mainly vertical upward flows above the rotor-stator region (in the cell) which are turned into tangential flows at the boundary of the froth layer. In addition there are turbulent circulating flows at the froth boundary." Thus, the flow in the flotation cell as a whole is a superposition of both directional and turbulent flows. Because of the existence of different types of flows in the flotation cell, the bubbles that are introduced into the cell for the purpose of aerating the pulp, as well as any bubble/particle aggregates which form, move in flows which are non-turbulent in some regions and highly turbulent in others. The entire situation is further complicated by the fact that not only is the actual bubble motion governed by the involved nature of the flow field in the flotation cell, but also by the reality of having to deal with bubble surfaces that

are not solid; in the limiting situation where the bubble is covered by an adsorption layer of surfactant, and is not too large, the bubble will behave (approximately) like a solid particle because of its quasi-rigid surface.

Other forces which contribute to the stability (instability) of a bubble/particle aggregate in the flotation cell are the force of gravity, the static buoyancy force of the immersed part of the bubble, the hydrostatic pressure of the liquid above the contact area of the particle at the fluid interface between the particle and bubble after formation of the three-phase contact (Fig. 2), the capillary force exerted on the three-phase contact, and the capillary pressure in the gas bubble which acts on the contact area of an attached particle. The ratio of detachment forces F_{det} to attachment forces F_{ad} which characterizes the stability of the aggregate turns out to be a (dimensionless) similarity parameter, which is analogous to the so-called Bond number (Schulze, [13]). The expression for P_{stab}, which is presented in §II, is based on this Bond number and is, in large measure, attributable to the recent experimental work of Plate [16].

Several authors have pointed out the often significant differences that exist between flotation deinking and mineral flotation. As Pan et al. [6] point out, "ink and toner particles are inherently very hydrophobic whereas pulp fibers are inherently hydrophilic, and so a necessary condition for flotation is more or less naturally met." Schulze [14] notes that in both mineral flotation and flotation deinking cells "more or less the same interaction processes should occur between floatable particles and air bubbles in a high turbulent field ... (so that) the microprocesses in flotation deinking cells are the same as in classical mineral flotation cells. But one of the features of flotation deinking is the presence of fibrous material of low density along with printing ink particles of usually small size and low density. In spite of the considerable degree of hydrophobicity of ink particles, their flotation recovery is by no means

as effective as the flotation of mineral particles where inertial forces play a dominant role in the interaction process with gas bubbles." Schulze [14] concludes that "the fundamental problems which we are confronted within flotation deinking are, therefore: the nonuniform, heterogeneous surface properties of ink particles with low weight and small size and the high density of stock suspension where fibers form a quasielastic network." Although we will not consider the issue of the high density of fibers in the pulp suspension, we will take into account, in the modelling of the various microprocesses, the issues related to the surface properties of ink particles and their relatively small size as compared with typical mineral particles.

II The Probability Distributions Associated with the Individual Elementary Processes.

The process of flotation deinking is a macroprocess composed of a large number of individual microprocesses that take place both simultaneously and successively in time and space in a flotation cell. As Schulze [5] has indicated: "drastic simplifications are necessary in the modelling of the flotation process in order to describe the overall process clearly." In this section, we focus our attention on describing the probability distributions which are associated with some of the key microprocesses. The various microprocesses to be considered will be described in the following order:

(i) the approach of an ink particle to a bubble in the flow field which exists in a neighborhood of that bubble and its possible interaction with the bubble.

(ii) the subsequent sliding motion of an ink particle on the surface of the thin liquid film that forms around the bubble, the rupture of this film at some critical thickness h_{crit}, and the almost immediate formation of a three-phase contact (TPC).

(iii) the stabilization (or destabilization) of the resultant bubble/particle aggregate with respect to the external stress forces that act on it.

A key element in a formulation of the kinetic equation (governing the evolution of the number of free ink particles per unit time in a given volume of the flotation cell), which will not be considered in this section, is a description of the number Z of bubble/particle collisions per unit time per unit volume; this particular issue will be addressed when we discuss the simplifying assumptions that are built into the model in §III.

i) Probability of Capture of an Ink Particle by a Bubble

We begin by noting that in this section all ink particles and all bubbles in any given volume of the flotation cell will be assumed to be perfectly spherical. As should be clear from Fig. 1, not all ink particles which move within the bubble projection domain of radius R_B can collide with or be intercepted by a bubble but, rather, only those within a so-called streaming tube of limiting capture radius R_c. The derivation of expressions for R_c depends mainly on the basic assumptions made about the relative sizes of the ink particle and the bubble, i.e., R_p vs. R_B, and, especially, about the nature of the flow field in which the ink particle moves. Many authors have noted that inertial forces play little or no role for ink particles, and, thus, the collision or interception probability of such particles is much lower than that of particles of normal (mineral-type) size because ink particles tend to follow, with little deviation, the fluid streamlines in the flow field around the bubble; such considerations are built into the expressions for P_c (which denotes the probability of capture of an ink particle by a bubble). Particle 'capture' by a bubble implies that a particle is close enough to a bubble to interact with it. Capture does not mean a bubble/particle aggregate has necessarily formed. Many authors have noted that capture efficiency depends both on particle and bubble size. The

probability of particle capture is higher the larger the particle size and the smaller the bubble size. A particular problem with respect to flotation deinking is the fact that air bubbles which are too small (about 0.1 mm according to Isler [17]) tend to adhere to fibers in a pulp suspension, while only bubbles larger than approximately 0.3 mm possess sufficient bouyancy to pass through the quasielastic fiber network in the suspension; such considerations will not concern us here.

Several key quantities arise in discussing the flow field in a neighborhood of a bubble and the ensuing expression for P_c; chief among them is the bubble Reynolds number Re_B:

$$Re_B = \frac{v_B d_B \rho_\ell}{\mu_\ell} \tag{II.1}$$

where v_B is the bubble rising velocity; $d_B = 2R_B$ is the bubble diameter; ρ_ℓ is the density of the liquid in a neighborhood of the bubble; and μ_ℓ is the dynamic viscosity of the liquid. Also of importance is the constant C_B employed by many authors (e.g., Schulze and co-workers [13-15]) to characterize the degree of bubble retardation (i.e., the degree to which a bubble has its surface covered with a surface-retarding chemical); this constant is chosen so that a completely retarded or rigid bubble corresponds to $C_B = 1$.

The other essential measure associated with the determination of the probability P_c is the so-called Stokes number. The Stokes number, which is the ratio of the inertia force of the (ink) particle to the viscous drag force of the bubble, is given by

$$St = \frac{\rho_p d_p^2 v_B}{9\mu_\ell d_B} \equiv \frac{Re_B \rho_p d_p^2}{9\rho_\ell d_B^2} \tag{II.2}$$

where $d_p = 2R_p$ and ρ_p is the particle density. In the literature on flotation processes it appears that the following criteria are generally accepted [13]:

(i) For $St > 1$, particle trajectories are, essentially, straight lines and most particles that attach to bubbles do so as the result of a genuine collision process.

(ii) For $0.1 < St < 1$, inertia forces play a role in any attachment process although actual impact collisions are still possible; because of the existence of the inertia force, particle trajectories will deviate slightly from the streamlines associated with the flow field around the bubble.

(iii) For $St << 0.1$, inertia forces no longer influence particle motion; there are basically no impact collisions possible between particles and bubbles and particles follow the streamlines in the flow around a bubble.

To make a determination of a form for P_c, we first define P_c to be the ratio of the number of particles with $R_p < R_B$ that encounter a bubble per unit time to the number of (ink) particles that approach a bubble in a stream tube with cross section equal to πR_B^2 (see, e.g., Fig. 1); computing the aforementioned ratio, we easily find that

$$P_c = (R_c/R_B)^2 \tag{II.3}$$

with R_c the capture radius as depicted in Fig. 1. The expression for P_c, which is given in (II.3), is deceptively simple because the elucidation of an expression for R_c is a far from trivial exercise which depends on the shape of particle trajectories in the fluid flow around the bubble, as well as the interactions which are possible between an (ink) particle and the bubble surface; these, in turn, depend on the mass and inertia of the particle and on the nature of the flow field in which both particle and bubble are immersed. In the literature it is assumed that a particle is acted on only by static buoyancy, inertial, gravitational, and drag forces; in other words, there are no centrifugal forces acting on the particle when it flows around the bubble, and the particle is assumed not to perturb the flow field around the bubble. Thus, at this stage of approach of an (ink) particle to a bubble, we consider only the long-range hydrodynamic interaction as opposed to the short-range hydrodynamic

interactions which must be taken into account when, e.g., a particle is engaged in sliding around the bubble over the thin liquid film which surrounds it. Consider, in Cartesian coordinates, the forces (and their components) which act on a particle as it approaches a single bubble in the flotation cell. If $\vec{v}_p$ represents the particle velocity with components v_{px} and v_{py} and m is the inertial mass of the particle (i.e., the actual particle mass m_p plus the fluid mass accelerated with it), then for an (ink) particle approaching a bubble, we have, in general,

$$\begin{cases} m\dfrac{dv_{py}}{dt} &= -F_{dy} \\ m\dfrac{dv_{px}}{dt} &= (F_g - F_b) - F_{dx} \end{cases} \tag{II.4}$$

where F_{dx} and F_{dy} represent the drag froces in the x and y directions, respectively, and $F_g - F_b$ is the difference between the gravitational and buoyancy forces which act on a particle as it approaches a single bubble in the flotation cell. We note that besides depending on ρ_p, ρ_ℓ, the dynamic viscosity μ_ℓ, R_p, etc., the expressions in (II.4) depend in a critical fashion on whatever form one assumes for the fluid velocity field $\vec{u}$. To be somewhat more precise, (II.4) can be written in the form

$$\frac{4}{3}\pi R_p^3 \rho_p \frac{dv_{px}}{dt} = -\frac{4}{3}\pi R_p^3 \Delta\rho g - 6\pi\mu_\ell R_p(v_{px} - u_x) \tag{II.5}$$

$$\frac{4}{3}\pi R_p^3 \rho_p \frac{dv_{py}}{dt} = 6\pi\mu_\ell R_p(u_y - v_{py}) \tag{II.6}$$

If (II.5), (II.6) are written in dimensionless form, then the key parameters which appear are the Stokes number St and G, the (dimensionless) particle settling velocity, (or gravity parameter) given by

$$G = \frac{2R_p^2(\rho_p - \rho_\ell)g}{9\mu_\ell v_B} \tag{II.7}$$

Expressions for the capture radius R_c are, thus, based on the solution of initial-value problems coupled with assumptions about the nature of the fluid flow field $\vec{u}$, the magnitudes of the

key parameters, and some information relative to the degree of retardation of the bubble surface. In fact, normal and tangential components of fluid flow across the bubble surface change their values depending on the degree of retardation. For a movable bubble ($C_B = 4$), it is known that [15]

$$u_r \sim \frac{z}{R_B}, \quad u_\phi = const. \tag{II.8}$$

where u_r, u_ϕ are, respectively, the radial and tangential components of the fluid velocity vector, and z is the distance from the surface of the bubble. For a rigid bubble,

$$u_r \sim \left(\frac{z}{R_B}\right)^2, \; u_\phi \sim \frac{z}{R_B} \tag{II.9}$$

Furthermore, in a Stokes flow (where, typically, $Re_B << 1$), $u_\phi = 0$ at $r = R_B$, with r measured from the center of the spherical bubble, while in the other extreme case, that of a potential flow (typically, $80 < Re_B < 500$), we have $u_\phi > 0$ at $r = R_B$. We now note the relevant relations which have been delineated in the literature for u_r and u_ϕ beginning with those associated with Stokes flow around the bubble: Dukhin et al. [18], quoting the work of Hadamard and Rybczynski, employ the relations

$$\begin{cases} u_{rs} &= -v_B \left(1 - \dfrac{(2\mu_\ell + 3\zeta)}{2(\mu_\ell + \zeta)} \dfrac{R_B}{r} + \dfrac{\zeta R_B^3}{2(\mu_\ell + \zeta) r^3}\right) \cos\phi \\ u_{\phi s} &= v_B \left(1 - \dfrac{(2\mu_\ell + 3\zeta)}{4(\mu_\ell + \zeta)} \dfrac{R_B}{r} - \dfrac{\zeta R_B^3}{4(\mu_\ell + \zeta) r^3}\right) \sin\phi \end{cases} \tag{II.10}$$

where ζ is a coefficient which depends on the mobility of the bubble surface. For $\zeta >> \mu_\ell$, (II.10) may be reduced to

$$\begin{cases} u_{rs} &= v_B \left(1 - \dfrac{3R_B}{2r} + \dfrac{R_B^3}{2r^3}\right) \cos\phi \\ u_{\phi s} &= v_B \left(1 - \dfrac{3R_B}{4r} - \dfrac{R_B^3}{4r^3}\right) \sin\phi \end{cases} \tag{II.11}$$

The relations (II.11) would hold, e.g., for a gas bubble in water. For $\zeta << \mu_\ell$ (the situation that results if there is a highly viscous dispersing agent in the water), (II.10) assumes the form

$$\begin{cases} u_{rs} &= -v_B \left(1 - \dfrac{R_B}{r}\right) \cos\phi \\ u_{\phi s} &= v_B \left(1 - \dfrac{R_B}{2r}\right) \sin\phi \end{cases} \tag{II.12}$$

On the other hand, for the case of a potential flow around the bubble surface, the radial and tangential components u_{rp}, $u_{\phi p}$ have the form

$$\begin{cases} u_{rp} &= -v_B \left(1 - \dfrac{R_B^3}{r^3}\right) \cos\phi \\ u_{\phi p} &= v_B \left(1 + \dfrac{R_B^3}{2r^3}\right) \sin\phi \end{cases} \tag{II.13}$$

However, in actual flotation machines, several authors have pointed out that an intermediate bubble Reynolds number with $1 < Re_B < 100$ often applies; e.g., Yoon and Luttrell [19] deduced the following expressions for the radial and tangential components of the velocity field $\vec{u}_*$ of the fluid:

$$\begin{cases} u_{*r} &= u_{rs} - v_B \dfrac{3Re_B^*}{2} \left(\dfrac{R_B^4}{r^4} - \dfrac{R_B^3}{r^3} - \dfrac{R_B^2}{r^2} - \dfrac{R_B}{r}\right) \cos\phi \\ u_{*\phi} &= u_{\phi s} + v_B \dfrac{3Re_B^*}{4} \left(\dfrac{R_B}{r} + \dfrac{R_B^3}{r^3} - \dfrac{2R_B^4}{r^4}\right) \sin\phi \end{cases} \tag{II.14}$$

where the components u_{rs}, $u_{\phi s}$ are given either by (II.11) for the case where $\zeta >> \mu_\ell$ or by (II.12) for the case where $\zeta << \mu_\ell$ and

$$Re_B^* = Re_B^{0.72}/15 \tag{II.15}$$

There do not appear to be expressions for the velocity field of the fluid which take into account the presence of turbulent wakes and which can be used in order to model the capture radius

R_c; however, many models do account for the presence of turbulence, in a later stage of the overall flotation process, i.e., in modelling the stability of a bubble particle aggregate.

We note that we are limiting our considerations here to the encounter between a single (ink) particle and a single bubble. An assemblage of bubbles and particles behaves much differently than a single bubble and particle (e.g., see Flint and Howarth, [20]) but no satisfactory treatment of the problem to describe R_c for this situation has been addressed in the open literature.

From the system of equations (II.5), (II.6) and associated initial conditions, coupled with the expressions delineated above for the fluid velocity field, estimates have been developed for the capture radius R_c, which, subsequently, have been employed in (II.3) so as to yield estimates for P_c. In this paper, we will limit ourselves only to those estimates which obtain in the case where the Stokes number St, as defined by (II.2), satisfies $St << 0.1$, for this is the situation which is most directly related to the one encountered in flotation deinking cells. Thus, according to Dukhin et al. [18] as well as Derjaguin et al. [21], Ahmed and Jameson [22], and Yoon and Luttrell [19], for intermediate Reynolds numbers in the range between 0.2 and 100, for rigid bubbles ($C_B = 1$), and bubble sizes up to 1 mm

$$P_c = \left(\frac{3}{2} + \frac{4Re_B^{0.72}}{15}\right)\frac{R_p^2}{R_B^2} \tag{II.16}$$

with the relation believed to be valid for particle sizes up to 100 μm. In Dukhin et al. [18] and Derjaguin et al. [21], we also find the relations

$$P_{cs} = \frac{3}{2}\left(\frac{R_p}{R_B}\right)^2 \tag{II.17}$$

for a Stokes flow situation around the bubble with $Re_B << 1$ and an (assumed) completely retarded bubble surface, while for a potential flow situation with $80 < Re_B < 500$ and a

completely unretarded bubble surface, they deduce that

$$P_{cp} = 3\left(\frac{R_p}{R_B}\right) \tag{II.18}$$

More refined results than those expressed by (II.16) - (II.18), which take into account the influence of the critical film thickness which must be obtained in order for the film 'surrounding' the bubble to rupture (thus, leading to the formation of a three-phase contact between (ink) particle, bubble, and fluid), have the form

$$\hat{P}_{cs} \cong 79.4\frac{R_p^2}{R_B^2}\left[6 - 2ln\left(\frac{h_{crit}}{R_p}\right)\right]^{-2} \tag{II.19}$$

for a Stokes flow around the bubble, assuming the bubble to be completely retarded, and

$$\hat{P}_{cp} \cong 1.78\frac{R_p}{R_B}\left(\frac{h_{crit}}{R_p}\right)^{0.123} \tag{II.20}$$

for a potential flow around the bubble surface with the assumption that the bubble is completely unretarded. We note that in as much as $h_{crit} \approx R_p$, in many situations encountered in flotation cells, the approximate relation (II.19) implies that

$$\hat{P}_{cs} \cong 2.2\left(\frac{R_p}{R_B}\right)^2 \tag{II.21}$$

Because the expressions for P_c depend on the degree of bubble retardation, which can be expected to be (at least) slightly different from bubble to bubble, as well as on the critical film thickness h_{crit}, the best that one can expect to do in trying to model the overall process, is to say that

$$P_c = \alpha_c\left(\frac{R_p}{R_B}\right)^2 \tag{II.22}$$

'on the average' where α_c will vary from bubble to bubble within any volume element. If, to a high degree of certainty we know that we are dealing, almost uniformly, with completely

retarded bubbles in a volume element within a flotation cell, then a reasonable estimate for α_c, is

$$\alpha_c \approx \frac{3}{2} + \frac{4Re_B^{0.72}}{15} \tag{II.23}$$

ii) Probability of Adhesion by Sliding

When a particle in a flotation cell approaches a bubble to within a close enough distance, so that capture is possible, two kinds of interaction may occur (i) an impact (collision) in which the surface of the bubble is strongly deformed - in which case an extended thin liquid film forms about the bubble and the particle is repelled, unless, during the first contact, attachment of the particle to the bubble takes place or (ii) sliding of the particle along the surface of the thin liquid film surrounding the bubble with a resultant weak surface deformation. In the latter case, which is the one most relevant for ink particles, whether or not particle attachment takes place depends in a crucial manner on the duration of the contact time of the particle with the liquid film surrounding the bubble in relation to the drainage time (i.e., induction time τ_i) of this film until its rupture; thus, the contact (or sliding) time of the particle $\tau_{s\ell}$ must be greater than or equal to τ_i.

The sliding process is the most complicated of all the microprocesses to model. To estimate the probability of adhesion by sliding $P_{as\ell}$, we must model, first of all, the particle motion in the flow field of the bubble as it slides (in an almost circular path) over the surface. We must also model the drainage and subsequent rupture of the liquid film that separates the particle from the bubble so as to be able to estimate the induction time τ_i. From the modelling of the sliding motion of the particle over the bubble surface, one may predict the positional angle ϕ as a function of film thickness h. Since attachment of an ink particle to a bubble must (see Fig. 1) take place in the angular range $\phi_T < \phi < \pi/2$ where

$\phi_T = \phi|_{t=0}$ is the 'touching angle,' a suitable nonnegative function of ϕ_T should serve as a measure of $P_{as\ell}$. One may deduce, using numerical computations, that the probability $P_{as\ell}$ depends strongly on h_{crit} (the film thickness just prior to film rupture), the assumptions one makes about the flow field around the bubble (potential, Stokes, or an intermediate flow), the degree of mobility of the bubble surface, the particle and bubble sizes, and the bubble rising velocity. The influence, in particular, of bubble rising velocity v_B on $P_{as\ell}$ is evident from the graphs in Fig. 3, which are reproduced from Schulze [13]. To simplify matters, the following assumptions have been made in the literature [13, 14]:

(i) the particles move in a quasistationary manner (i.e., inertial forces are negligible) on an almost circular path across the bubble surface.

(ii) the sliding path L is much greater than the film thickness h, and, moreover, it is assumed that $dL/dt > dh/dt$.

(iii) in the domain $0 < \phi < \pi/2$, the influence of the flow boundary layer is negligible, especially in the case of movable or unretarded bubbles.

(iv) the tangential component of the fluid flow can, as in the computation of P_c, be modeled in the case of an unretarded bubble by potential flow and in the case of a completely retarded bubble by the intermediate flow of Yoon and Luttrell, op.cit.

Insert Fig. 3

A force balance governs the sliding motion of the particle; however, while a complete set of equations can be derived from the imposition of balance of forces (gravitational, centrifugal, flow force, lifting force, and drag force), the solution of the associated initial value problems can only be found numerically [6].

As a consequence of assumptions (i)-(iv), delineated above, it follows that (see, e.g., Schulze [13]) the particle tangential velocity satisfies

$$v_{p\phi} \equiv \frac{dL}{dt} = u_\phi + v_{ps} \sin \phi \tag{II.24}$$

where the particle settling velocity v_{ps} is given by

$$v_{ps} \equiv Re_p \mu_\ell / 2\rho_\ell R_p \tag{II.25}$$

Some typical values for v_B and v_{ps} are given in Table 1 with the particle 'Reynolds number' defined as follows: Let

$$Ar \equiv 8R_p^3 \Delta\rho g / \nu_\ell^2 \rho_\ell \tag{II.26}$$

be the Archimedes number, where $\nu_\ell = \mu_\ell / \rho_\ell$. Then,

$$\begin{cases} Re_p = Ar/18, & \text{for } Ar < 9 \\ Re_p = \left(\dfrac{Ar}{13.9}\right)^{0.7143}, & \text{for } 9 < Ar < 82,500 \end{cases} \tag{II.27}$$

Insert Table 1

In polar coordinates, balance of forces in the radial direction reads (see Fig. 4):

$$-F_{gr} - F_{ur} + F_T + F_c + F_L = 0 \tag{II.28}$$

with

$$F_{gr} = \frac{4}{3}\pi R_p^3 \Delta\rho g \cos\phi \tag{II.29}$$

being the component of the (apparent) particle weight in the radial direction,

$$F_T = 6\pi\mu_\ell R_p^2 v_{pr} / (hC_B) \tag{II.30}$$

being the resistive force generated during the drainage of the liquid film surrounding the bubble surface (which is estimated by using the theory of capillary hydrodynamics for thin

films),

$$F_c = 4\pi R_p^3 \Delta\rho v_{p\phi}^2/3r \tag{II.31}$$

being the centrifugal force acting on the sliding particle which (by assumption) moves on a circular path with $r = R_B + R_p + h$,

$$F_{ur} \cong 6\pi\mu_\ell R_p |u_r| \tag{II.32}$$

being the 'flow force' that acts on a sliding particle close to the bubble wall, and

$$F_L \cong 3.24\mu_\ell R_p v_{prel}\sqrt{Re_S} \tag{II.33}$$

being the driftage or lift force acting on the particle, where

$$v_{prel} = u_\phi - v_{ps\phi} \tag{II.34}$$

and

$$Re_S = 4SR_p^2\rho_\ell/\mu_\ell \tag{II.35}$$

is the Reynolds number of shear for the flow around the bubble surface. The relation (II.33) has been established, e.g., in Clift et al. [23]. In (II.35), S is the shear gradient, i.e., $S = \dfrac{\partial u_\phi}{\partial r}$, which for a potential flow over the bubble surface has the form

$$S_{pot} = v_B\left(-\frac{3R_B^3}{2r^4}\right)\sin\phi \tag{II.36}$$

and for an intermediate flow is

$$S_{int} \equiv v_B\left[\left(\frac{3R_B}{4r^2} + \frac{3R_B^3}{4r^4}\right) + \frac{3}{4}Re_B^*\left(-\frac{R_B}{r^2} - \frac{3R_B^3}{r^4} + \frac{8R_B^4}{r^5}\right)\right]\sin\phi \tag{II.37}$$

Insert Fig. 4

For balance of forces in the tangential direction, we have

$$F_{g\phi} - F_{w\phi} = 0 \tag{II.38}$$

where

$$F_{g\phi} = \frac{4}{3}\pi R_p^3 \Delta\rho g \sin\phi \tag{II.39}$$

is the component of the (apparent) particle weight in the tangential direction, and $F_{w\phi}$, which is strongly dependent on the flow field, as well as the degree to which the bubble surface is covered with surface-retarding molecules, is the drag force acting on the moving particle. According to Goldman et al. [24], for a completely retarded bubble with $\left(\frac{h}{R_p}\right) > 10^{-3}$,

$$F_{w\phi} \cong \frac{16}{5}\pi\mu_\ell v_{p\phi} R_p ln\left(\frac{h}{R_p}\right) \tag{II.40}$$

For an unretarded bubble in a potential flow, most authors set $F_{w\phi} = 0$. By manipulating (II.24) - (II.40), we obtain the system of equations

$$\frac{d\phi}{dt} = \frac{1}{r}\left[\frac{v_{ps}\ \sin\phi}{\lambda}\right] \tag{II.41}$$

$$\frac{dh}{dt} = -hC_B(g_0\cos\phi + \frac{|u_r|}{R_p} - \frac{g_1 v_{p\phi}^2}{r} - g_2 v_{prel}\sqrt{Re_S}) \tag{II.42}$$

with

$$\begin{cases} g_0 &= 2\Delta\rho g R_p/9\mu_\ell \\ g_1 &= 2\Delta\rho R_p \\ g_2 &= 0.1714/R_p \end{cases} \tag{II.43}$$

and

$$\lambda = \frac{8}{15}\left|ln\left(\frac{h}{R_p}\right)\right| \tag{II.44}$$

where $\phi(t)$ gives the location along the bubble surface, at time t, for the particle with touching angle $\phi_T = \phi(0)$, and $h(t)$ is the height of the disjoining film above that point on the bubble

surface at the same time t. An analysis of (II.41), (II.42) shows that this system is of the form

$$\frac{d\phi}{dt} = F_1(\phi, h) \tag{II.45}$$

$$\frac{dh}{dt} = F_2(\phi, h) \tag{II.46}$$

The associated initial conditions are $\phi(0) = \phi_T$, $0 < \phi_T < \pi/2$, and according to Dukhin and Rulev [25],

$$h(0) = h_0 \equiv 2R_p(3\mu_\ell v_{pr}/8\sigma C_B)^{1/2}. \tag{II.47}$$

By eliminating the time variable from (II.45), (II.46), we can write the equation for the particle trajectory as

$$\frac{dh}{d\phi} = F_2(\phi, h)/F_1(\phi, h) \equiv F(\phi, h) \tag{II.48}$$

For $h > R_p$, it may be deduced (Goren [26]) that (II.48) implies that the particle trajectory coincides with a streamline of the fluid flow around the bubble surface, if the separation between the particle surface and the bubble surface is larger than the particle radius R_p. From (II.48) and the (initial) condition that $h = h(0) \equiv h_0$, for $\phi = \phi(0) \equiv \phi_T$, one may obtain (at least, numerically) a solution $h = h_T(\phi)$ that can be inverted so as to produce the associated functional relation $\phi = \phi_T(h)$. Our interest lies in being able to compute ϕ^*_{crit}, which is the largest value of ϕ_T such that h_{crit} is reached in the interval $\phi_T < \phi < \pi/2$; the thickness h_{crit} just prior to the rupture of the thin liquid film surrounding the bubble surface must be determined experimentally.

A simple derivation of (II.30) may be obtained from the work of Derjaguin et al. [27]; it depends on the following considerations, which are based on Fig. 5, showing the formation of the thin film between the particle and the bubble surface with the resultant weak deformation of the latter: using ideas from the capillary hydrodynamics of thin films, one assumes that

the average pressure p in the film depends only on the radial distance x (in Fig. 5) and is responsible for the resultant weak deformation of the bubble surface. At any point of the surface, we have

$$p(x,t) = P_\sigma(x,t) \tag{II.49}$$

where P_σ is the capillary pressure caused by the deformation of the bubble surface. In general,

$$P_\sigma = \frac{\sigma}{x}\frac{\partial}{\partial x}\left(x\frac{\partial h_1}{\partial x}\right) \tag{II.50}$$

where we assume that h_1 depends weakly on time and where σ is the surface tension; $h_1(x)$ measures the warping of the bubble surface at x, and it is assumed that $\frac{\partial h_1}{\partial x} << 1$. The Navier-Stokes equation specialized to the thin film reads

$$\mu_\ell \frac{\partial^2 u}{\partial y^2} = \frac{\partial p}{\partial x} = \frac{\partial P_\sigma}{\partial x} \tag{II.51}$$

where $u(y)$ is the efflux velocity (component) which is directed along the bubble surface. As boundary conditions, we have

$$u\left(\hat{h} + \frac{x^2}{2R_p}\right) = 0, \ \frac{\partial u}{\partial y}(-h_1) = 0 \tag{II.52}$$

with $\hat{h}$ being the distance between the particle and the nondeformed bubble surface (which is assumed to be flat if the particle is much smaller than the bubble), while $x^2/2R_p$ is the constant curvature of the particle surface. From (II.51), (II.52), one obtains

$$u(y) = \frac{1}{\mu_\ell}\frac{\partial P_\sigma}{\partial x}\left[\frac{y^2}{2} + h_1 y - \frac{1}{2}\left(\hat{h} + \frac{x^2}{2R_p}\right)^2 - h_1\left(\hat{h} + \frac{x^2}{2R_p}\right)\right] \tag{II.53}$$

Insert Fig. 5

For $h_1(x)$, Derjaguin et al., [27] obtain the equation

$$\frac{\partial^3 h_1}{\partial x^3} + \frac{1}{x}\frac{\partial^2 h_1}{\partial x^2} - \frac{1}{x^2}\frac{\partial h_1}{\partial x} = \frac{3}{2}\frac{\mu_\ell v_{pr}}{\sigma} f(x) \tag{II.54}$$

with

$$f(x) = x\left(h_1(0) + \hat{h} + \frac{x^2}{2R_p}\right)^{-3} \tag{II.55}$$

and the associated boundary data

$$\left.\frac{\partial h_1}{\partial x}\right|_{x=0} = 0, \quad \left.\frac{\partial h_1}{\partial x}\right|_{x\to\infty} = 0 \tag{II.56}$$

From (II.54), (II.56), we find that

$$\frac{\partial h_1}{\partial x} = \frac{3}{4}\frac{\mu_\ell v_{pr}}{\sigma} R_p \left\{ -\frac{R_p}{h^*} + \frac{x^2}{2(h^* + \frac{x^2}{2R_p})^2} + R_p \left[\frac{2}{(h^* + \frac{x^2}{2R_p})^2} - \frac{h^*}{(h^* + \frac{x^2}{2R_p})^2} \right] \right\} \tag{II.57}$$

with $h^*(x) = h_1(0) + \hat{h}(x)$. For the resistive (or drag) force generated during the drainage of the liquid film surrounding the bubble, in the sliding process, we have, by (II.57),

$$\begin{aligned} F_T = \iint_{S_B} P_\sigma dS_B &= \int_0^\infty P_\sigma 2\pi x \, dx \\ &= 2\pi\sigma \int_0^\infty \frac{\partial}{\partial x}(x\frac{\partial h_1}{\partial x})dx \\ &= 2\pi\sigma x \left.\frac{\partial h_1}{\partial x}\right|_0^\infty \\ &= \frac{6\pi\mu_\ell R_p^2 v_{pr}}{4(h_1 + \hat{h})} \end{aligned} \tag{II.58}$$

which is (II.30) with $C_B = 4$.

The critical film thickness, h_{crit}, is determined by the dynamics of the so-called disjoining film between the particle and the bubble; disruption of this film is controlled by nonhydrodynamic interactions and forces such as London-Van der Waals dispersion forces, which act to create a normal force in the disjoining film. This latter interaction is represented by the disjoining pressure, which can be shown to be proportional to h^{-3}, with the constant of

proportionality a multiple of the Hamaker constant. As Pan et al. [12] note, "any region of the disjoining film which is thinner than another region will experience a greater internal pressure. This greater pressure will, in turn, tend to drive fluid from the thinner region, causing further thinning, and, since the dispersion forces are attractive, eventual rupture." If we consider a nondraining thin film with constant, homogeneous density and fluid viscosity, then the following relations apply [1], where x now represents arc length measured along the coordinate surface, while y measures distance normal to the particle surface (Fig. 6):

(i) $\dfrac{\partial u}{\partial x} + \dfrac{\partial v}{\partial y} = 0$, where (u, v) is the velocity field of the thin disjoining film

(ii) Equation (II.51) and $\dfrac{\partial P_\sigma}{\partial y} = 0$, where P_σ is the disjoining pressure.

(iii)
$$P_\sigma = -\sigma \frac{\partial^2 h}{\partial x^2} + \frac{A}{h^3} - \frac{B e^{-\kappa h}}{1 - e^{-\kappa h}} \tag{II.59}$$

which generalizes (II.50) in that it accounts not only for the surface (interfacial) tension but also for London-Van der Waals dispersion and electrostatic interactions (with B related to the strength of the electrostatic interactions and $1/\kappa$ the double layer thickness).

(iv) The kinematic condition at the film interface:

$$\frac{\partial h}{\partial t} = v - u \frac{\partial h}{\partial x} \quad (\text{at } y = h) \tag{II.60}$$

and the boundary conditions:

(v) At the solid/film interface, i.e., $y = 0$ in Fig. 6, $u = 0$, while at the film/bubble interface, i.e., at $y = h$, either (a) $\tau_{xy} = 0$, signifying a completely free mobile surface or (b) a tangentially immobile surface with τ_{xy} large and $u = 0$ or (c) conditions which

result from having a surface tension σ, which is not constant but is, rather, a function of position x. For now, we will assume the film/bubble interface to be completely unretarded and will comment, below, on the situation mentioned in (b) and (c).

Insert Fig. 6

The conditions in (i)-(v), above, (see, e.g., Williams and Davis [28]) lead to the following nonlinear partial differential equation for the film thickness $h(x,t)$:

$$\frac{\partial h}{\partial t} = \frac{1}{3\mu_\ell}\frac{\partial}{\partial x}\left[h^3\left(\frac{\partial P_\sigma}{\partial x}\right)\right] \tag{II.61}$$

For the disjoining film model, with constant surface tension, and the case of a free, mobile bubble/film interface, if we assume that electrostatic interactions are negligible (i.e., $B = 0$ in (II.59)) and then substitute from (II.59) into (II.61), we obtain

$$\frac{\partial h}{\partial t} = \frac{1}{3\mu_\ell}\frac{\partial}{\partial x}\left[h^3\frac{\partial}{\partial x}\left(-\sigma\frac{\partial^2 h}{\partial x^2} + \frac{A}{h^3}\right)\right] \tag{II.62}$$

to which we must append an appropriate initial condition for $h(x,t)$. As shown in the Appendix, both (II.54) and (II.62) are just different local coordinate realizations of the same partial differential equation when $A = 0$. The results indicated above are based on the no-slip or free bubble/film interface boundary condition, and various differences are noted if one uses the tangentially immobile interface condition instead; the main result to be noted is that the rupture time is, on the average, four times greater for the rigid bubble as compared with the free bubble. Paulsen et al. [1] illustrate the relationship between the predicted disjoining film rupture time and basic input parameters of the model, namely, the initial bubble/particle separation (which is controlled by the hydrodynamics of the situation), the Hamaker constant A and surface tension σ (which are determined by the surface science and physical chemistry of the system), and an (initial) perturbation wavelength.

It is often necessary to generalize the disjoining film model to account for variable surface tension σ. As noted by Paulsen et al. [1], "if a surfactant is present in the continuous, liquid phase below its critical micelle concentration, its surface concentration along the disjoining film/bubble interface can act to change the surface tension. Surface tension gradients along the interface cause tangential forces known as the Marangoni effect." At the interface, the relevant boundary condition for the variable σ takes the form

$$\frac{\partial \sigma}{\partial x} = -\mu_\ell \frac{\partial u}{\partial y} \quad (y = h) \tag{II.63}$$

and, in place of (II.61), we have

$$\frac{\partial h}{\partial t} = \frac{1}{3\mu_\ell} \frac{\partial}{\partial x} \left[h^3 \left(\frac{\partial P_\sigma}{\partial x} \right) + \frac{3h^2}{2} \left(\frac{\partial \sigma}{\partial x} \right) \right] \tag{II.64}$$

To (II.64), an appropriate initial condition for $h(x,t)$, the boundary condition (II.63) at $y = h$, and the boundary condition $u = 0$ at $y = 0$, we now append a (linear) representation for σ of the form

$$\sigma = \sigma_0 + M\Gamma \tag{II.65}$$

where $M = \sigma'(\Gamma)$ is assumed constant; σ_0 is the surface tension of the liquid phase in the absence of added surfactant; and Γ is the surface concentration of surfactant; then, a transport equation for Γ is formulated in the form

$$\frac{\partial \Gamma}{\partial t} = D_s \frac{\partial^2 \Gamma}{\partial x^2} - \frac{\partial}{\partial x}(u_s \Gamma) \tag{II.66}$$

with u_s the velocity component of u restricted to the interface (surface) and D_s the diffusion coefficient. The (constitutive) relation (II.65) can now be used to eliminate σ from (II.64) and (II.59), thus leading to a system of evolution equations for the film thickness $h(x,t)$ and the surface concentration of surfactant $\Gamma(x,t)$. At the film/bubble interface at $y = h$,

the kinematic relation (II.60) and the (boundary) condition (II.63) must be satisfied, where (u, v) is the two-dimensional velocity field of the disjoining liquid film between the particle and the bubble; we must, of course, also specify an initial surfactant surface concentration Γ_0 as well as an initial condition for h. Several authors [1, 5] have postulated a mean initial thickness for the disjoining film of $\bar{h}_0$ and then assumed that with $\bar{\epsilon}$ a small perturbation, and λ a characteristic wavelength (of the order of magnitude of R_p),

$$h_0 = \bar{h}_0 \left(1 + \bar{\epsilon} \cos\left(\frac{2\pi x}{\lambda}\right)\right) \tag{II.67}$$

with $\bar{h}_0/\lambda << 1$, i.e., that the particle and bubble have advanced to within a distance $\bar{h}_0$ of each other, so that nonhydrodynamic interactions become important, and that (at $t = 0$) a perturbation then causes local thinning of the disjoining film. Numerical studies based on the system of equations delineated above, and the assumption of a uniform initial surface concentration, may be found in [1] where the authors show that it is possible to follow the change in surfactant concentration and its effect on the position along the film surface at which rupture occurs.

Schulze [15] cites the following experimental result, which correlates the degree of particle hydrophobicity with h_{crit}:

$$h_{crit} = 23.3[\sigma(1 - \cos\theta_A)]^{0.16} \tag{II.68}$$

where θ_A is the advancing contact angle. We must be careful, however, if we want to apply the empirical result (II.68): in the earlier paper [14], the empirical result presented for h_{crit} is given as

$$h_{crit} = 16.6[\sigma(1 - \cos\theta_A)]^{0.22} \tag{II.69}$$

Indeed, Schulze notes [15] that the result (II.68) "has been obtained for a particular case. It cannot be used generally for calculations of the critical thickness."

We are now in a position to formulate an expression for the probability of adhesion by sliding $P_{as\ell}$. With reference to Fig. 1, it is assumed that at time $t = 0$ the ink particle touches or makes contact with the disjoining film surrounding the bubble surface; we set the value of the position angle ϕ at $t = 0$ equal to ϕ_T (the "touching angle"). The distance of the center of the ink particle from the stagnation line through the center of the bubble when position angle $\phi = \phi_T$ is denoted by R_T. The essential idea behind the formulation of the classical expression for $P_{as\ell}$ is this: attachment of an ink particle to a bubble is possible if the critical film thickness h_{crit} is reached during sliding for a position angle ϕ in the range $\phi_T < \phi < \pi/2$. As incoming ink particles, which are to have any chance of attachment must contact the disjoining film with a touching angle ϕ_T between $\phi_T = 0$ and $\phi_T = \pi/2$, the larger ϕ_T can be, with attachment during the sliding process possible, the greater the probability of adhesion by sliding; with this in mind, we define the critical position angle ϕ^*_{crit} to be the largest touching angle ϕ_T that may be used as an initial condition in the system (II.41), (II.42) so that $h = h_{crit}$ will be reached at a position angle ϕ_{crit} (see Fig. 7) in the range $\phi_T < \phi_{crit} < \pi/2$, i.e.,

$$\begin{aligned} \phi^*_{crit} \quad &= \max \{\phi_T = \phi(0) | h_{crit} = h(\phi_{crit}), \\ &\qquad \text{for some } \phi_{crit},\ \phi_T < \phi_{crit} < \pi/2\} \end{aligned} \tag{II.70}$$

Insert Fig. 7

Thus, let us assume that for a particular set of conditions (i.e., given C_B, v_B, R_p, R_B, etc.) we have determined, experimentally, an empirical relation of the type (II.68) or (II.69) for the critical film thickness h_{crit}. From the system (II.41), (II.42), we determine a solution, with $\phi(0) = \phi_T$, and $h(0) = h_0$, in the form $h = h_T(\phi)$, where the T subscript denotes the dependence of the functional relationship on the choice of ϕ_T; we must then attempt to determine the largest value of ϕ_T such that the graph of $h_T(\phi)$ will intersect the line $h = h_{crit}$

for a ϕ in the range $\phi_T < \phi < \pi/2$. The situation is depicted schematically in Fig. 8 following a similar figure in Schulze [15]; the largest value of ϕ_T that yields an intersection of $h_T(\phi)$ with the line $h = h_{crit}$ for $\phi_T < \phi < \pi/2$ is, by definition, ϕ^*_{crit}. Finally, the probability of adhesion through the sliding process is defined as follows:

$$P^T_{as\ell} = \frac{R_T^2}{(R_B + R_p)^2} \tag{II.71}$$

However,

$$R_T = r_T \sin\phi_T \cong (R_B + R_p)\sin\phi_T \tag{II.72}$$

so with $\phi_T = \phi^*_{crit}$

$$P_{as\ell} = P^T_{as\ell}\Big|_{\phi_T = \phi_{crit}} \equiv \sin^2\phi^*_{crit} \tag{II.73}$$

Insert Fig. 8

From the numerical results in Schulze [15], it is known that $P_{as\ell}$ (i) increases as R_B decreases, (ii) increases as v_B decreases, (iii) decreases as R_p increases, especially for values of R_p which are small, (iv) increases as C_B increases, and (v) increases as h_{crit} increases. Also, the smaller the relative velocity between the particles and the bubbles during the interaction, the longer the sliding time and the greater the probability of attachment by sliding become. As an illustration of the kind of results that may be obtained by using solutions of the system (II.41), (II.42), and the definition (II.73), we show (in Fig. 3) the figure from Schulze [13], which depicts for both the case of an intermediate flow with $C_B = 1$ as well as for the case of a potential flow with $C_B = 4$, the probability of adhesion by sliding, $P_{as\ell}$, as a function of R_p, v_B, and h_{crit}; among the conclusions that follow is the fact that the main influence on P_{asl} is the bubble size as manifested by the real bubble-rising velocity v_B: $P_{as\ell}$ is greater with smaller R_B mostly because of the smaller associated value of v_B. A summary of some

results relative to the magnitudes of the various forces which act on sliding particles under intermediate flow conditions is given in Table 2, which is reproduced from Schulze [15].

Insert Table 2

iii) Probability of Extension of the Three-Phase Contact

After the rupture of the thin liquid film which surrounds a bubble, a sufficiently large three-phase contact (TPC) between the film, particle, and bubble (see, Fig. 2) must be formed in a sufficiently short time τ_{tpc}. As Schulze [13] has noted, "the formation of the primary hole during the rupture of the thin film takes place in the microsecond or even nanosecond range and it is therefore not so important for the kinetics of the flotation process ... the probability of the further TPC expansion is important and depends on many influencing factors, above all, the dynamics of dewetting. The driving power for both the enlargement of the hole and the expansion of three-phase contact is the difference of the interface energies ... given by the difference between the instant value of the dynamic receding contact angle θ_R^* and the receding contact angle of equilibrium $\theta_{SR\infty}$."

The importance of the time interval τ_{tpc} is this: within the flotation cell external stress forces will exert themselves on bubble/particle aggregates as a consequence of the existence of turbulent vortices; the formation of a sufficiently large TPC in a sufficiently short time τ_{tpc} is required so that a requisite strong force of attachment will exist to prevent dissolution of the aggregate. As a consequence of these considerations, for stable attachment after film rupture, we must have $\tau_{tpc} < \tau_v$ where τ_v is an average lifetime for turbulent vortices within the flotation cell; the average lifetimes for laminar and nonlaminar vortices have been estimated (Liepe [29], Albring [30]) as follows:

(i) for laminar vortices: $\tau_v \equiv \tau_{v\ell} \simeq 0.6 r_v^2/\nu_\ell$ with ν_ℓ the (liquid) kinematic viscosity and

$r_v \approx R_B + R_p$

(ii) for nonlaminar vortices: $\tau_v \equiv \tau_{vn\ell} \simeq 13 r_v^{2/3}/\epsilon^{1/3}$ with ϵ the mean (Kolmogorov) energy dissipation in the flotation cell.

It has also been shown (Scheludko et al. [31]) that the velocity of expansion of the (assumed circular) hole of radius r_p after the rupture of the thin liquid film surrounding the bubble is given by

$$\frac{dr_p}{dt} = a_{tpc}\sigma(\cos\theta_R^* - \cos\theta_{sR\infty}) \tag{II.74}$$

where a_{tpc} is the so-called instantaneous mobility coefficient of the TPC, which, in general, will itself depend on the current value of r_p and which has been shown, experimentally, to depend in a very complicated fashion on the surface properties of the liquid film as well as on all the external and frictional forces which act on the TPC. For these reasons, it is common practice to use a constant mean value for a_{tpc}. Scheludko et al. [31] have estimated that

$$\tau_{tpc} \approx R_p^2\sqrt{(2\Delta\rho g/3)/[a_{tpc}\sigma^{3/2}(1-\cos\ \theta_{SR\infty})]} \tag{II.75}$$

For the probability of successful extension of the three-phase contact Schulze [13] assumes an exponential distribution which, in its simplest form may be approximated as

$$P_{tpc} \approx 1 - exp\left(-\frac{\tau_v}{\tau_{tpc}}\right) \tag{II.76}$$

In most of the elementary kinetic or population models that have been formulated prior to this study, P_{tpc} does not enter into the product of individual probabilities that constitutes the relevant kinetic constants because P_{tpc} is, consistently, to within 1%, equal to one over a wide range of particle sizes for particles with a smooth boundary. Tables 3 (taken from Schulze [13]) and 4 (Schulze [32]) provide some information on the magnitudes of the individual probabilities for bubble/particle formation and stability.

Insert Table 3

Insert Table 4

iv) Probability of Aggregate Stability

Whenever the attachment that has formed between an ink particle and a bubble is stronger than the sum of all the external stress forces which act on the aggregate, the bubble/particle aggregate remains a stable entity on its journey to the froth layer. To compute the probability P_{stab} of bubble/particle aggregate stability, it is necessary to consider the force balance that applies to the ink particles at the liquid/bubble interface; this force balance (Fig. 9) includes the force of gravity exerted on the ink particle (i.e., the weight of the particle), the static buoyancy force, the hydrostatic pressure force, the capillary force which is exerted on the three-phase contact line, the capillary pressure in the air bubble itself that is exerted onto the contact area between the particle and the bubble, and an additional detaching force due to the acceleration a_c which the particle experiences in the turbulent flow field of the flotation cell. An extended analysis of the force balance that affects aggregate stability has been carried out by many authors (see, in particular, Schulze [13] and Hou and Hui [33], and the references cited therein) with the following mathematical expressions for the z, or vertical components of the individual forces that are involved:

(i) For the gravitational force F_g that acts on the ink particle (assumed to be spherical),

$$F_g = \frac{4}{3}\pi R_p^3 \rho_p g \tag{II.77}$$

(ii) For the static buoyancy force that acts on the immersed portion of the particle,

$$F_b = \frac{\pi}{3} R_p^3 \rho_\ell g[(1-\cos\omega)^2(2+\cos\omega)] \tag{II.78}$$

where ω is the angle in the particle, which is clearly indicated in Fig. 2. Some authors (e.g., Hou and Hui [33]) make the simplifying assumption that the entire particle is immersed in the liquid, which is equivalent to setting $\omega = \pi$ in (II.78); in this case, (II.78) simplifies to

$$\tilde{F}_b = \frac{4}{3}\pi R_p^3 \rho_\ell g \tag{II.79}$$

so that grouping (II.77) and (II.79) together leads to an expression for the apparent weight F_{wt} of the ink particle, namely,

$$F_{wt} = \frac{4}{3}\pi R_p^3 (\rho_p - \rho_\ell)\, g \tag{II.80}$$

(iii) For the hydrostatic pressure of the liquid of height z_0 above the contact area of radius r_p (where $r_p = R_p \sin\psi = R_p \sin\omega$ in Fig. 2),

$$F_{hyd} = \pi R_p^2 (\sin^2\omega) \rho_\ell g z_0 \tag{II.81}$$

(iv) For the capillary force exerted on the three-phase contact in the z-direction,

$$F_{ca} = -2\pi R_p \sigma \sin\omega \sin(\omega + \theta) \tag{II.82}$$

where θ is the contact angle.

(v) For the force generated by the capillary pressure in the gas bubble that acts on the contact area of the attached (spherical) ink particle,

$$F_\sigma = \pi r_p^2 P_\sigma \approx \pi R_p^2 \sin^2\omega \left(\frac{2\sigma}{R_B} - 2R_B \rho_\ell g\right) \tag{II.83}$$

and

(vi) For the additional detaching force that is due to the acceleration experienced in the turbulent external flow field in the flotation cell,

$$F_d = \frac{4}{3}\pi R_p^3 \rho_p a_c \tag{II.84}$$

where expressions for the acceleration field a_c depend on both the structure and the intensity of the turbulent flow field, in particular, on the energy dissipation ϵ in a given volume element of the flotation cell. For aggregates where the particle size is smaller than the bubble size, it has been determined [13] that

$$a_c \approx 1.9\epsilon^{2/3}/(R_B + R_p)^{1/3} \tag{II.85}$$

in the inertial region of the vortex, while for even smaller aggregates in the dissipation region of a vortex flow,

$$a_c \approx 0.52\epsilon^{3/4}/\nu_\ell^{1/4}. \tag{II.86}$$

Insert Fig. 9

For the special case that is often realized in column flotation, where the bubble may flow laminarly, a_c in a first approximation depends only on the tangential motion of the particle as it moves across the bubble surface

$$a_c \approx (u_\phi + v_{ps\phi})^2/(R_B + R_p) \tag{II.87}$$

If, in (II.87), we use the approximation that is valid for a completely unretarded bubble in a potential flow, namely, $u_\phi \approx \frac{3}{2} v_B \sin\phi$, then (II.87) becomes

$$a_c \approx \left[\left(\frac{3}{2}v_B + v_{ps}\right)\sin\phi\right]^2/(R_B + R_p) \tag{II.88}$$

We may simplify (II.88) even further by using only the maximum value which occurs at $\phi = \pi/2$, i.e.,

$$a_c^{max} \approx (\frac{3}{2}v_B + v_{ps})^2/(R_B + R_p) \tag{II.89}$$

Remarks: The precise computation of the force balance associated with determining the stability of bubble/particle aggregates is complicated by an incomplete knowledge of terms like z_0. Using the theory of capillary menisci (Schulze [5], Scheludko et al. [34]), $z_0 = z_0(R_p)$ may be obtained by numerical integration of the Laplace equation arising in that theory (Huh and Scriven [35]); this equation is known to have no analytical solution. Schulze [5] credits Huh and Scriven [35] with the first complete numerical solution for bounded menisci and indicates that the approach considering unbounded menisci simplifies the mathematical treatment, and is easily justified in those cases where $R_p << R_B$. By an unbounded menisci, we mean one in which the direction associated with r_p in Fig. 2 is not bounded by a solid wall or influenced in any other way; this corresponds to the case of a particle at an infinitely extended interface.

Among the observations which have been made that lead to a simplification of the analysis of the force balance that controls the stability of bubble/particle aggregates are the following (e.g., Schulze [13]):

(i) For contact angles $\theta < \pi/2$ and particles with $R_p < 150\mu m$, it may be estimated that the hydrostatic pressure of the liquid above the contact area of radius r_p is negligible, i.e., $F_{hyd} \approx 0$.

(ii) The maximum value of the remaining force of attachment, the capillary force F_{ca} exerted at the three-phase contact, occurs when $\omega = \omega^* \approx \pi - \frac{1}{2}\theta$.

Now let $F_{ad} = F_{ca} + F_{hyd}$ denote the sum of the attachment forces, that $F_{det} = F_g - F_b + F_d + F_\sigma$ denotes the sum of the forces that lead to detachment. If we characterize the stability of the bubble/particle aggregate by the ratio,

$$Bo' \equiv \frac{F_{det}}{F_{ad}} = \frac{F_g - F_b + F_d + F_\sigma}{F_{ca} + F_{hyd}}, \tag{II.90}$$

a dimensionless similarity parameter similar to the so-called Bond number (Schulze [13]), use the expression (II.79) in lieu of (II.78) for the buoyancy force F_b, the assumption that $F_{hyd} \approx 0$, and, in place of F_{ca}, use the maximum value F_{cam} at $\omega = \omega^*$, we obtain the approximate relation

$$Bo' \approx \frac{4R_p^2(\Delta\rho g + \rho_p a_c) + 3R_p \sin^2\omega^* f(R_B)}{|6\sigma \sin\omega^* \sin(\omega^* + \theta)|} \tag{II.91}$$

where

$$f(R_B) = \left(\frac{2\sigma}{R_B} - 2R_B\rho_\ell g\right) \tag{II.92}$$

Following the experiments of Plate [16], a reasonable form for the probability of aggregate stability is

$$P_{stab} = 1 - exp\left[-\left(\frac{F_{cam} - F_{det}}{F_{det}}\right)\right] \tag{II.93}$$

where

$$F_{cam} = 2\pi\sigma R_p \sin\left(\pi - \frac{\theta}{2}\right) \sin\left(\pi + \frac{\theta}{2}\right) \tag{II.94}$$

or in view of the definition (II.90),

$$P_{stab} = 1 - exp\left(1 - \frac{1}{Bo'}\right). \tag{II.95}$$

As a direct consequence of (II.90) and (II.95), we may conclude that:

(i) As $F_{det} \to 0$, $Bo' \to 0$, and $P_{stab} \to 1$

(ii) For $F_{det} < F_{cam}$, $Bo' < 1$, so $0 < P_{stab} < 1$

(iii) For $F_{det} = F_{cam}$, $Bo' = 1$, and $P_{stab} = 0$

We reproduce in Fig. 10 a figure from Schulze [13] which is based on (II.90), (II.95) and shows the probability of stability of bubble/particle aggregates as a function of particle size R_p, contact angle θ, and mean energy dissipation ϵ. Other experimental verifications of the expression (II.95) have been published by Crawford and Ralston [36]. Using essentially the same definitions of the individual detachment and attachment forces as Schulze [13], Hou and Hui [33] have studied the effects of varying the particle size R_p, the bubble size R_B, the contact angle θ, and the surface tension σ; parametric values for test cases in [33] were chosen so as to correspond to the case of carbon black ink particles. The work in [33] is based on the Fowkes [37] relation between contact angle, surface tension, and surface energy.

Insert Fig. 10

v) Summary of the Basic Results

In §III we delineate a kinetic model for the evolution of the number of free ink particles in a volume element of a flotation cell; this model involves two 'kinetic' constants: k_1 - which governs the overall probability of a free ink particle successfully intercepting and adhering to an air bubble and forming a stable aggregate with that bubble, and k_2 - which measures the probability that a bubble/particle aggregate (pair) will destabilize and split off a new (free) ink particle. The kinetic (constant) k_1 is given by

$$k_1 = Z P_c P_{as\ell} P_{tpc} P_{stab} \tag{II.96}$$

while for k_2, we will have

$$k_2 = P_{destab} \equiv 1 - P_{stab}. \tag{II.97}$$

In §III, we will discuss some of the results that are applicable for computing Z, the 'collision' frequency (or number of bubble/particle collisions per unit time in a unit volume of the flotation cell).

We now summarize the basic expressions for the individual microprocess probabilities that enter into (II.96) and (II.97).

1) For the probability of capture of an ink particle by a bubble, we assume P_c to be given by (II.22), i.e.,

$$P_c = \alpha_c (R_p/R_B)^2 \tag{II.22}$$

where for intermediate Reynolds numbers between 0.2 and 100, an assumed rigid bubble, and bubble sizes of up to 1mm, α_c has the (approximate) value in (II.23).

2) For $P_{as\ell}$, the probability of adhesion of an ink particle to a bubble through the sliding process, we have (II.73), i.e.,

$$P_{as\ell} = \sin^2 \phi^*_{crit} \tag{II.73}$$

where ϕ^*_{crit} is defined by (II.70), namely,

$$\phi^*_{crit} = \max \{\phi_T = \phi(0) | h_{crit} = h(\phi_{crit}), \text{ for some } \phi_{crit}, \phi_T < \phi_{crit} < \pi/2\} \tag{II.70}$$

with ϕ_T the touching angle and h_{crit} the requisite film thickness in the (disjoining) film between the particle and the bubble that is needed for film rupture. The quantity h_{crit} is to be determined experimentally. To use (II.70), we must 'integrate' the system (II.41), (II.42) to obtain h as a function of the position angle ϕ for the given initial conditions $h_0 = h(0)$ and $\phi(0) = \phi_T$. By varying ϕ_T, we then have to try to determine

the largest value of $\phi(0) = \phi_T$ consistent with being able to solve $h_{crit} = h(\phi)$ for a $\phi = \phi_{crit}$ in the range $\phi_T < \phi_{crit} < \pi/2$.

3) For P_{tpc}, the probability of extension of the three-phase contact we avail ourselves of the fact that computations (see, Table 3) clearly indicate that $P_{tpc} \simeq 1.0$ to within 1% over a wide range of particle sizes, provided the particle boundaries are idealized to be smooth.

4) For P_{stab}, the probability that a formed bubble/particle aggregate (pair) will remain stable on its journey into the froth layer we have the expression (II.95), i.e.,

$$P_{stab} = 1 - exp\left(1 - \frac{1}{Bo'}\right) \tag{II.95}$$

where the modified Bond number is given by (II.91) and (II.92) with $w^* \approx \pi - \theta/2$, and a_c is given either by (II.85) in the inertial region of a (turbulent) vortex, (II.86) in the dissipation region of a (turbulent) vortex, or (II.87) for the more or less laminar-type conditions that seem to be prevalent in column flotation.

In view of (II.97),

$$k_2 \equiv P_{destab} \equiv exp\left(1 - \frac{1}{Bo'}\right) \tag{II.98}$$

so that as $Bo' \to 0$, $k_2 \to 0$. If we set $P_{tpc} \approx 1$ use (II.96), (II.22), (II.73), and (II.95) and combine $P_c, P_{as\ell}$, and P_{stab}, we obtain

$$k_1 = Z\alpha_c \left(\frac{R_p}{R_B}\right)^2 \sin^2 \phi^*_{crit} \left[1 - exp\left(1 - \frac{1}{Bo'}\right)\right] \tag{II.99}$$

where Z, the collision frequency will be elaborated in §III. In spite of the fact that the physical parameters, i.e., $R_p, R_B, v_B, \epsilon, \sigma$, etc., enter into the determination of all the probability functions which mediate the individual microprocesses, the analytical disparity between the

way in which these parameters enter the expressions for the individual probabilities does not allow for any major analytical simplification in the expressions for the kinetic constants k_1 and k_2.

III A Population Balance-Type Model and Its Predictions.

In this section we construct a model for studying the evolution of the number of free ink particles in a unit volume of the flotation cell; the model is based on a number of simplifying assumptions which are delineated below.

i) Basic Simplifying Assumptions

a) Collision Frequency

Because of the low interception probability that governs the interaction between small particles (such as ink particles) and air bubbles, efforts are often made to increase the collision frequency Z by increasing the intensity of turbulence in the flow field surrounding the bubble; in doing this, however, one must be cognizant of the fact that increasing the turbulence intensity in the flow regime also has the effect of helping to destabilize a bubble/particle aggregate once one has formed. A frequently used model for the collision frequency Z in flotation cells is the one attributed to Abrahamson [38], to wit

$$Z = 5 n_p n_B \left(\frac{d_p + d_B}{2} \right)^2 \sqrt{\bar{v}_p^2 + \bar{v}_B^2} \tag{III.1}$$

with n_p and n_B being the number of particles and bubbles, respectively, per unit volume of the flotation cell, while $\bar{v}_p$ and $\bar{v}_B$ are, respectively, the mean relative velocities of the

particles and the bubbles in the flow field. According to the work of Liepe and Möckel [39], these mean relative velocities vary with the turbulent energy dissipation ϵ:

$$\sqrt{\bar{v}_p^2 + \bar{v}_B^2} = \frac{2^{7/9}}{3} \frac{\epsilon^{4/9}}{\nu_\ell^{1/3} \rho_\ell^{2/3}} \sqrt{R_B^{14/9} (\Delta\rho_B)^{4/3} + R_p^{14/9} (\Delta\rho_p)^{4/3}} \tag{III.2}$$

where $\Delta\rho_B = \rho_B - \rho_\ell$ and $\Delta\rho_p = \rho_p - \rho_\ell$.

Combining (III.1) with (III.2), we are led to the following expression for the collision frequency Z:

$$Z = C_z n_p n_B \frac{\epsilon^{4/9}}{\nu_\ell^{1/3} \rho_\ell^{2/3}} (R_p + R_B)^2 \sqrt{R_B^{14/9} (\Delta\rho_B)^{4/3} + R_p^{14/9} (\Delta\rho_p)^{4/3}} \tag{III.3}$$

where $C_z = 2^{7/9}\frac{5}{3}$. The analysis that produces (III.3) is not universally accepted, so, e.g., the work of Camp and Stein [40] leads to the expression

$$Z = \frac{4}{3} \left(\frac{\epsilon}{\nu_\ell}\right)^{1/2} (R_p + R_B)^3 n_p n_B, \tag{III.4}$$

for the number of bubble/particle collisions per unit volume of the flotation cell, while that of Saffman and Turner [41] produces

$$Z = \left(\frac{8\pi}{15}\right)^{1/2} \left(\frac{\epsilon}{\nu_\ell}\right)^{1/2} (R_p + R_B)^3 n_p n_B \tag{III.5}$$

In the last two cases delineated above, what emerges is an expression for Z of the form

$$Z = k_Z n_p n_B \tag{III.6}$$

with

$$k_Z = \Gamma_Z (R_p + R_B)^\lambda \epsilon^\gamma \tag{III.7}$$

for some constant of proportionality Γ_Z, which includes material properties, and some (positive) constants λ and γ. As a rule, given the complicated nature of the flow field in a typical

flotation cell, one may work with the general form

$$Z = \Gamma_Z \epsilon^\gamma n_p n_B f\left(R_p, R_B; \Delta\rho_p, \Delta\rho_B\right) \tag{III.8}$$

and then determine, empirically, for the situation in question, the values of Γ_Z, γ, and the functional form of f. In the modelling which leads, e.g., to an expression like (III.1), all possible collisions of all particles and bubbles present in a unit volume of the turbulent flow field are taken into account. However, in the course of applying an expression like (III.1) to the specific process of flotation deinking, it may be more appropriate to use not n_p, the total number of ink particles in a unit volume of the flotation cell at time t, but, rather, n_p^f - the number of free ink particles in a unit volume of the flotation cell at time t.

b) The Number of Bubbles and Ink Particles in a Control Volume per Unit Time

An arbitrary unit volume $\mathcal{V}_f$ in the flotation cell, with boundary $\partial\mathcal{V}_f$, is assumed for the model development. We denote by $n_p(t)$ the total number of ink particles (both free and attached) in $\mathcal{V}_f$ at time t, by $n_B(t)$ the total number of bubbles (both free as well as with ink particles attached to them) in $\mathcal{V}_f$ at time t, by $n_p^f(t)$ the number of free ink particles present in $\mathcal{V}_f$ at time t, by $n_p^a(t)$ the number of ink particles in $\mathcal{V}_f$ at time t which are attached to bubbles in $\mathcal{V}_f$, by $n_B^f(t)$ the number of bubbles in $\mathcal{V}_f$ at time t which have no ink particles attached to them, and by $n_B^a(t)$ the number of bubbles in $\mathcal{V}_f$ at time t which have one or more ink particles attached to them. Clearly, for any $t > 0$,

$$\begin{cases} n_p(t) = n_p^f(t) + n_p^a(t) \\ n_B(t) = n_B^f(t) + n_B^a(t) \end{cases} \tag{III.9}$$

and

$$n_p^a(t) \geq n_B^a(t) \tag{III.10}$$

In general, if $\bar{\lambda}(t)$ denotes an average number of ink particles at time t, in the volume element $\mathcal{V}_f$, which are attached to bubbles in $\mathcal{V}_f$, that have ink particles attached to them,

$$n_p^a(t) = \bar{\lambda}(t) n_B^a(t) \tag{III.11}$$

In general, bubbles that have ink particles attached to them in $\mathcal{V}_f$ will have more than one ink particle attached as they move up toward the froth layer, with the number of ink particles attached to a particular bubble varying with time (as well as from bubble to bubble); in any case, it may be expected that the average measure $\bar{\lambda}(t)$ introduced above will satisfy $\dot{\bar{\lambda}}(t) \neq 0$, as well as $\bar{\lambda}(t) \geq 1$ for all $t > 0$. Also because of convection and diffusion of both ink particles and bubbles, both into as well as out of the volume element $\mathcal{V}_f$, it is to be anticipated that both $\dot{n}_B(t) \neq 0$ and $\dot{n}_p(t) \neq 0$. We assume, here, for the sake of simplicity, that

$$\text{(a)} \quad n_p(t) = n_p \text{ (const.), for } t > 0 \tag{III.12}$$

$$\text{(b)} \quad n_B(t) = n_B \text{ (const.), for } t > 0 \tag{III.13}$$

$$\text{(c)} \quad \bar{\lambda}(t) = 1, \text{ for } t > 0. \tag{III.14}$$

We also assume in this first model that

$$\text{(d)} \quad n_B \geq n_p \tag{III.15}$$

Now, set $\gamma(t) = n_p^f(t)/n_p$, so that $0 \leq \gamma(t) \leq 1$, for all $t > 0$, and

$$n_p^f(t) = \gamma(t) n_p \tag{III.16}$$

i.e., $\gamma(t)$ represents the fraction of all ink particles at time t, in $\mathcal{V}_f$, which are free so that

$$n_p^a(t) = (1 - \gamma(t)) n_p \tag{III.17}$$

In a similar fashion we set $\zeta(t) = n_B^f(t)/n_B$, so that $0 \leq \zeta(t) \leq 1$, for all $t > 0$, and

$$n_B^f(t) = \zeta(t) n_B, \tag{III.18}$$

i.e., $\zeta(t)$ represents the fraction of all bubbles at time t, in $\mathcal{V}_f$, which are free so that

$$n_B^a(t) = (1 - \zeta(t)) n_B \tag{III.19}$$

Then, by virtue of (III.11),

$$(1 - \gamma(t)) n_p = \bar{\lambda}(t)(1 - \zeta(t)) n_B \tag{III.20}$$

and, in view of (III.14),

$$\frac{n_p}{n_B} = \frac{1 - \zeta(t)}{1 - \gamma(t)}, \text{ all } t > 0 \tag{III.21}$$

The ideal goal in a flotation deinking apparatus would be that, for each volume element $\mathcal{V}_f$,

$$\gamma(t) \to 0, \text{ as } t \to \infty \tag{III.22}$$

or

$$n_p^a(t) \to n_p, \text{ as } t \to \infty \tag{III.23}$$

From (III.21), however, it follows that if $\gamma(t) \to 0$, as $t \to \infty$, then

$$n_p = n_B - \left(\lim_{t \to \infty} \zeta(t) \right) n_B \tag{III.24}$$

or

$$\lim_{t \to \infty} \zeta(t) = \frac{n_B - n_p}{n_B} \geq 0 \tag{III.25}$$

Using (III.24) in (III.18), it then follows that if $\gamma(t) \to 0$, as $t \to \infty$,

$$\begin{aligned} \lim_{t \to \infty} n_B^f(t) &= (\lim_{t \to \infty} \zeta(t)) n_B \qquad \text{(III.26)} \\ &= n_B - n_p \\ &= n_B - n_p^a \text{ (as } n_p^f(t) \to 0, \text{ for } t \to \infty) \\ &= n_B - n_B^a \text{ (for } \bar{\lambda} \equiv 1). \end{aligned}$$

ii) The Differential Equation Governing the Evolution of the Number of Free Ink Particles

Models for the evolution of the number of particles in a volume element of a flotation cell, which are of a kinetic-or population growth-type, go back, at least, to the work of Sutherland [9]; particularly noteworthy in this regard is the paper of Woodburn [4]. The book by Schulze [5] contains numerous references to elementary mathematical models of the flotation process, with most of them directly related to mineral flotation processes instead of flotation deinking.

Schulze [5] is careful to point out that the "generalized transport Balance equation for flotation is still unsolved since it contains terms which cannot be expressed explicitly yet"; he presents as the generalized transport balance equation for flotation an equation of the form

$$-\frac{\partial}{\partial t}(m_v\mu_i) = div[m_v\mu_i\,\vec{v_i}] - div[D_i \text{ grad } (m_v\mu_i)] - G_i \qquad \text{(III.27)}$$

where $\frac{\partial}{\partial t}(m_v\mu_i)$ is the change with time of the mass of the i-th particle class in the volume element under consideration; m_v is the total particle mass in the volume element; μ_i is the mass fraction of the i-th class in the volume element; $m_v\mu_i\,\vec{v_i}$ is the convective flow of mass of the i-th class in the volume element; $\vec{v_i}$ is the transport velocity of the i-th class in the volume element; D_i is the diffusion coefficient of the i-th class in the volume element; D_i grad $(m_v\mu_i)$ is the diffuse mass flow of the i-th class in the volume element; and G_i is the change of mass due to aggregate formation or destruction.

In flotation deinking we have $i = 1, 2$ with $i = 1$ referring to free ink particles and $i = 2$ referring to ink particles that adhere to bubbles; alternatively, $i = 1$ might refer to free ink particles in a unit volume of the flotation cell, while $i = 2$ would refer to bubbles in the unit volume under consideration that are either free or have ink particles adhering to them. To date the models we are aware of (except for [11]) ignore all terms on the right-hand

side of the general system (III.27) and, in addition, degenerate to a single equation (i.e., $i = 1$) for the evolution of free ink particles; also, the expression for the surviving term G_1, on the right-hand side of (III.28), is limited so as to represent only mass changes due to aggregate formation with aggregate destruction being ignored. Thus, Schulze [13, 14] writes the evolution equation in the form

$$\frac{dn_p^f}{dt} = -Zn_p^f n_B P_c P_a P_{stab} \tag{III.28}$$

where P_a represents the probability of adhesion ($P_a = P_{asl}P_{tpc}$). Missing from (III.28) is an expression to account for the generation of free ink particles as a consequence of the destruction of previously formed aggregates; this situation is remedied below where we make use of the hypotheses reflected in the assumptions (III.12)-(III.15).

We begin by writing the kinetic equation in the form

$$\frac{dn_p^f}{dt} = -k_1 n_p^f n_B^f + k_2 n_B^a \tag{III.29}$$

where the 'kinetic' constants k_1 and k_2 are the positive numbers given, respectively, by relations (II.96) and (II.97); the presence of n_B^f reflects the assumption that only a bubble with no ink particle attached is free to capture an ink particle. This assumption will be modified in future work.

We now return to (III.29); using the fact that, at time t, $n_B^f = n_B - n_B^a$, we obtain

$$\frac{dn_p^f}{dt} = -k_1 n_B n_p^f + k_1 n_p^f n_B^a + k_2 n_B^a \tag{III.30}$$

However, from (III.11), with $\bar{\lambda}(t) = 1$, $n_B^a = n_p^a$, so

$$\frac{dn_p^f}{dt} = -k_1 n_B n_p^f + n_p^a(k_1 n_p^f + k_2) \tag{III.31}$$

Into (III.31) we insert the fact that for all $t > 0$, $n_p^a = n_p - n_p^f$, in which case

$$\frac{dn_p^f}{dt} = -k_1(n_p^f)^2 + [k_1(n_p - n_B) - k_2]n_p^f + k_2 n_p \tag{III.32}$$

We now avail ourselves of (III.16); with $(\cdot) = \frac{d}{dt}(\ \ )$, (III.32) yields

$$\dot{\gamma}(t) = -(k_1 n_p)\gamma^2(t) + [k_1(n_p - n_B) - k_2]\gamma(t) + k_2 \tag{III.33}$$

Next, we set

$$\alpha \equiv n_p - n_B < 0, \tag{III.34}$$

the strict inequality in (III.34) reflecting the strong form of the hypothesis (III.15), and

$$A \equiv k_1 n_p > 0, \ \ B \equiv \alpha k_1 - k_2 < 0, \ \ C \equiv k_2 > 0 \tag{III.35}$$

We also replace, $\gamma(t)$ by $-\gamma(t) \equiv \Gamma(t)$, in (III.33), in which case

$$\dot{\Gamma}(t) = A\Gamma^2(t) + B\Gamma(t) - C \tag{III.36}$$

with the associated initial condition

$$\Gamma(0) = -\gamma(0) \equiv -\frac{n_p^f(0)}{n_p} \tag{III.37}$$

To transform (III.36) to a more manageable form, we write

$$\dot{\Gamma}(t) = A[(\Gamma(t) + \frac{B}{2A})^2 - (\frac{B^2}{4A^2} + \frac{C}{A})] \tag{III.38}$$

As $\frac{B^2}{4A^2} + \frac{C}{A} > 0$, there exists $\mu > 0$ such that

$$\frac{B^2}{4A^2} + \frac{C}{A} = \mu^2$$

in which case, if we set

$$y(t) \equiv \Gamma(t) + \frac{B}{2A} \tag{III.39}$$

then (III.38) becomes

$$\dot{y}(t) = A[y^2(t) - \mu^2], \ t > 0 \tag{III.40}$$

with the associated initial condition

$$y(0) = -\frac{n_p^f(0)}{n_p} + \frac{B}{2A} \tag{III.41}$$

If $y^2(t) > \mu^2$, for all $t > 0$, then as $A > 0$, we must have $\dot{y}(t) > 0$, for all $t > 0$, which, in turn, is equivalent to $\dot{\gamma}(t) < 0$, for all $t > 0$.

Remarks: In view of the definitions of A, B, and C, we have

$$y(t) = -\frac{n_p^f(t)}{n_p} + \frac{[(n_p - n_B)k_1 - k_2]}{2n_p k_1} \tag{III.42}$$

and

$$\mu = \sqrt{\frac{[(n_p - n_B)k_1 - k_2]^2}{4n_p^2 k_1^2} + \frac{k_2}{n_p k_1}} \tag{III.43}$$

while

$$y(0) \equiv y_0 = \frac{(n_p - n_B)k_1 - k_2}{2n_p k_1} - \frac{n_p^f(0)}{n_p} \tag{III.44}$$

As $k_1, k_2 > 0$, and $n_p < n_B$, we must have $y_0 < 0$.

iii) Integration of the Basic Model Equation

Subject to hypotheses (III.12)-(III.15), the evolution of the number of free ink particles in the unit volume element $\mathcal{V}_f$ is governed by the initial value problem (III.40), (III.41). The (positive) 'kinetic' constants k_1 and k_2 are defined in terms of the 'collision' frequency Z of particles and bubbles in $\mathcal{V}_f$ and the probabilities P_c, P_{asl}, P_{tpc}, and P_{stab} governing the individual microprocesses in the flotation deinking macroprocess; expressions for P_c, P_{asl}, P_{tpc}, and P_{stab} are summarized in (II.22), (II.73), (II.76), and (II.95); thus, k_1 and k_2 may be determined in terms of all the measurable or computable basic parameters of the flotation process, namely, R_p, $R_B, \theta, \epsilon, \sigma, \rho_\ell, \rho_p, \nu_\ell, h_{crit}$, etc.

Because (III.40) is a separable, first-order equation, its integration may be carried out explicitly so as to yield

$$\frac{1}{2\mu} ln \left| \frac{z-\mu}{z+\mu} \right| \Bigg]_{y_0}^{y(t)} = At, t > 0 \tag{III.45}$$

We now make the tentative assumption that $y^2(t) > \mu^2$, for all $t \geq 0$. Then, in lieu of (III.45), we have

$$ln \left[\left(\frac{y(t)-\mu}{y(t)+\mu} \right) \Big/ \left(\frac{y_0-\mu}{y_0+\mu} \right) \right] = 2\mu At \tag{III.46}$$

for all $t \geq 0$, from which it follows, with

$$\beta_0 = \frac{y_0-\mu}{y_0+\mu} \tag{III.47}$$

that

$$y(t) = \mu \frac{1+\beta_0 e^{2\mu At}}{1-\beta_0 e^{2\mu At}}, \; t \geq 0 \tag{III.48}$$

As $k_1 > 0$, $k_2 > 0$, and $n_p < n_B$, we have $y_0 < 0$ so, with μ the positive number given by (III.43), $y_0 - \mu < 0$. We want a condition which will guarantee that $y_0 + \mu < 0$ so that β_0, as given by (III.47), will satisfy $\beta_0 > 0$. To this end, we note that as $A > 0$ and $B < 0$

$$y_0 + \mu = -\gamma(0) - \frac{|B|}{2A} + \mu \tag{III.49}$$

But

$$\mu = \sqrt{\frac{B^2}{4A^2} + \frac{C}{A}} > \frac{|B|}{2A} \tag{III.50}$$

So (III.49) and (III.50) imply that

$$y_0 + \mu > -\gamma(0) \tag{III.51}$$

On the other hand,

$$\mu < \frac{|B|}{2A} + \sqrt{\frac{C}{A}} \tag{III.52}$$

so that

$$y_0 + \mu < -\gamma(0) + \sqrt{\frac{C}{A}} \tag{III.53}$$

Therefore,

$$-\gamma(0) < y_0 + \mu < -\gamma(0) + \sqrt{\frac{C}{A}} \tag{III.54}$$

where by (III.37), $\gamma(0) = \dfrac{n_p^f(0)}{n_p} > 0$. It then follows from (III.54) that for $\sqrt{\dfrac{C}{A}} < \gamma(0)$, i.e., for

$$\sqrt{\frac{k_2}{n_p k_1}} < \frac{n_p^f(0)}{n_p}$$

we have $y_0 + \mu < 0$. To the list of hypotheses (a)-(d), i.e., (III.12)-(III.15), we now add the following condition on the number of (initially) free particles in the volume element $\mathcal{V}_f$:

$$\text{(e)} \qquad \frac{n_p^f(0)}{\sqrt{n_p}} > \sqrt{\frac{k_2}{k_1}} \tag{III.55}$$

We also note that as $y_0 < 0$,

$$\beta_0 = \frac{|y_0| + \mu}{|y_0| - \mu} \tag{III.56}$$

Thus, as $\beta_0 > 0$, and $\mu > 0$, we must have $|y_0| > \mu$, in which case $\beta_0 > 1$.

To this point, we have shown that if $y^2(t) > \mu^2$, for all $t > 0$, integration of the initial-value problem (III.40), (III.41) leads to the expression (III.48) for $y(t)$, where β_0, as defined by (III.47), is strictly positive whenever (III.55) is satisfied. Using (III.48), we compute that

$$\dot{y}(t) = \frac{4\mu\beta_0 e^{2\mu A t}}{(1 - \beta_0 e^{2\mu A t})^2} \tag{III.57}$$

As $\beta_0 > 1$, $1 - \beta_0 e^{2\mu A t} \neq 0$, for all t, and, therefore, as a consequence of (III.57), we have $\dot{y}(t) > 0$, for all t. Using (III.48) and (III.57), it is an easy exercise to show that $y(t)$ satisfies (III.40) and (III.41). By local uniqueness for the solution of the initial-value problem, $y(t)$ as given by (III.48), is the solution of (III.40), (III.41). Thus, $y(t)$ satisfies

$$\frac{\dot{y}(t)}{A} = y^2(t) - \mu^2, \text{ for all } t > 0 \tag{III.58}$$

However, $\dot{y}(t) > 0$, for all t, while $A > 0$, and, therefore, the unique solution of the initial-value problem (III.40), (III.41) must conform to the hypothesis that $y^2(t) > \mu^2$, for all $t \geq 0$, provided condition (e) is satisfied.

iv) Some Predictions of the Basic Model

The fact that the solution (III.48) of the initial-value problem (III.40), (III.41) satisfies $y^2(t) > \mu^2$, for all $t \geq 0$, can be used to derive an interesting relationship among $n_B^f(t)$, $n_p^f(t)$, $n_p^a(t)$, and the ratio of the kinetic constants k_2/k_1. In fact, from the definition of $y(t)$, i.e.,

$$y(t) = -\frac{n_p^f(t)}{n_p} + \frac{B}{2A}$$

and (III.43), which is equivalent to

$$\mu = \sqrt{\frac{B^2}{2A^2} + \frac{k_2}{n_p k_1}} \tag{III.59}$$

we find that $y^2(t) > \mu^2$ $(\forall t \geq 0)$ is equivalent to

$$n_f^f(t) \left[\frac{n_p^f(t)}{n_p} - \frac{B}{A} \right] > \frac{k_2}{k_1} \tag{III.60}$$

Using the definitions of A and B, and recalling that $\alpha = n_p - n_B$, (III.60) becomes

$$n_p^f(t) - \alpha > \frac{k_2}{k_1} \left(\frac{n_p}{n_p^f(t)} - 1 \right) \tag{III.61}$$

But, $n_p^f(t) - \alpha = n_p^f(t) - (n_p - n_B) = n_B - n_p^a(t)$, or $n_p^f(t) - \alpha = n_B^f(t)$, as $n_p^a(t) = n_B^a(t)$. Thus, (III.61) implies that

$$n_B^f(t) > \left(\frac{k_2}{k_1} \right) \left(\frac{n_p^a(t)}{n_p^f(t)} \right), \; t \geq 0 \tag{III.62}$$

Thus, under hypotheses (a) - (e), the ratio, at time t, of the number of free ink particles in $\mathcal{V}_f$ to the number of attached ink particles in $\mathcal{V}_f$ is greater than the ratio of k_2/k_1 times the

inverse of the number of free bubbles in $\mathcal{V}_f$ at time t. Because $n_B^f(t) < n_B$, in $\mathcal{V}_f$, at any $t \geq 0$, we may also conclude from (III.62) that we have the lower bound

$$\frac{n_p^f(t)}{n_p^a(t)} > \left(\frac{k_2}{k_1}\right)\frac{1}{n_B} \tag{III.63}$$

As $n_p > n_p^f(t)$, at any time $t \geq 0$ in $\mathcal{V}_f$, it is clear that (III.63) implies that

$$n_p^a(t) < \left(\frac{k_1}{k_2}\right) n_p n_B, \; t \geq 0 \tag{III.64}$$

which provides an upper bound for the number of ink particles that attach themselves to bubbles in the volume element $\mathcal{V}_f$. We now write the solution (III.48), to the initial value problem (III.40), (III.41), in the form

$$\gamma(t) = \mu \left[\frac{1 + \frac{1}{\beta_0}e^{-2\mu A t}}{1 - \frac{1}{\beta_0}e^{-2\mu A t}}\right] - \frac{|B|}{2A} \tag{III.65}$$

from which it follows, in view of (III.35), that

$$\lim_{t\to\infty} \gamma(t) = \mu - \frac{(k_2 - [n_p - n_B]k_1)}{2n_p k_1} \tag{III.66}$$

Substituting for μ from (III.43) and recalling the definition of $\gamma(t)$, we obtain the following explicit form for the asymptotic limit of the number of free ink particles in $\mathcal{V}_f$:

$$\lim_{t\to\infty} \frac{n_p^f(t)}{n_p} = \sqrt{\frac{([n_p - n_B]k_1 - k_2)^2}{4n_p^2 k_1^2} + \frac{k_2}{n_p k_1}} - \frac{(k_2 + [n_B - n_p]k_1)}{2n_p k_1} \tag{III.67}$$

with the 'kinetic' constants k_1 and k_2 given by (II.96) and (II.97), respectively. The asymptotic limit in (III.67) may be simplified by approximating the right-hand side of (III.67). As

$$\mu - \frac{|B|}{2A} = \sqrt{\frac{B^2}{4A^2} + \frac{C}{A}} - \frac{|B|}{2A},$$

for $\frac{C}{A} \equiv \frac{k_2}{k_1 n_p}$ small, (the expected situation) the mean value theorem yields

$$\sqrt{\frac{B^2}{4A^2} + \frac{C}{A}} - \frac{|B|}{2A} \simeq \left(\frac{1}{2\sqrt{x}} \Big|_{x=\frac{B^2}{4A^2}} \right) \left(\frac{C}{A} \right) = \frac{C}{|B|} \tag{III.68}$$

so that

$$\lim_{t\to\infty} \frac{n_p^f(t)}{n_p} \simeq \frac{k_2}{k_2 + (n_B - n_p)k_1} \tag{III.69}$$

We may write (III.69) in the form

$$\lim_{t\to\infty} n_p^f(t) \simeq n_{p,\infty}^f \tag{III.70}$$

with

$$n_{p,\infty}^f \equiv \frac{k_2 n_p}{k_2 + (n_B - n_p)k_1} \tag{III.71}$$

so that the asymptotic limit $n_{p,\infty}^f$ is predicted to be independent of the initial number $n_p^f(0)$ of free particles in $\mathcal{V}_f$.

Directly from the expression for $\gamma(t)$, and the fact that $\beta_0 > 0$, $A > 0$, we have

$$\dot{\gamma}(t) = \frac{-4\mu^2 A \beta_0 e^{2\mu A t}}{(\beta_0 e^{2\mu A t} - 1)^2} < 0 \tag{III.72}$$

for all $t > 0$, so that the graph of $\gamma(t) = n_p^f(t)/n_p$ is monotonically, strictly decreasing for all $t > 0$. Furthermore,

$$\ddot{\gamma}(t) = 8\mu^3 A^2 \beta_0 e^{2\mu A t} \left[\frac{\beta_0 e^{2\mu A t} + 1}{(\beta_0 e^{2\mu A t} - 1)^3} \right] > 0 \tag{III.73}$$

so that the graph of $\gamma(t)$ is convex for all $t > 0$; the initial slope of the graph of γ is given by

$$\dot{\gamma}(0) = \frac{-4\mu^2 A \beta_0}{(\beta_0 - 1)^2} < 0 \tag{III.74}$$

By substituting from (III.47) into (III.74), and then replacing A, y_0, and μ by (the first relation in) (III.35), (III.44), and (III.43), respectively, an algebraic expression may be obtained for the initial rate of decrease of the number of free particles in the volume element $\mathcal{V}_f$,

i.e., for $\dot{n}_p^f(0)$, in terms of n_p, n_B, k_1, and k_2; a further substitution in the resulting expression for k_1 and k_2 from (II.96) and (II.97) yields an algebraic expression for $\dot{n}_p^f(0)$ in terms of $n_p, n_B, Z, P_c, P_{asl}, P_{tpc}$, and P_{stab}. Finally, by substituting for the collision frequency Z, and the individual probabilities that govern the various microprocess events in the flotation cell, we may obtain an algebraic expression for the initial rate of decrease of the number of free ink particles in $\mathcal{V}_f$ in terms of the basic parameters of the flotation process, i.e., $n_p, n_B, \rho_p, \rho_\ell, \epsilon, R_p, R_B, \sigma, \theta, \nu_\ell, h_{crit}, v_B$, etc.

Using the information in (III.72)-(III.74) and (III.69), the graph of $\gamma(t)$ depicted in Fig. 11 follows. On this graph $\gamma_\infty = (n_{p,\infty}^f/n_p)$ is the asymptotic limit for large t, of $n_p^f(t)/n_p$; $\bar{\gamma}(t)$ is the graph of the tangent line to $\gamma(t)$ at $t = 0$, i.e.,

$$\bar{\gamma}(t) = \frac{-4\mu^2 A\beta_0}{(\beta_0 - 1)^2}t + \frac{n_p^f(0)}{n_p}, \tag{III.75}$$

$\bar{t}$ is the time at which the graph of $\bar{\gamma}(t)$ intersects the asymptote $\gamma = \gamma_\infty$, i.e.,

$$\bar{t} = \frac{\left(\frac{n_p^f(0)}{n_p}\right) - \gamma_\infty}{4\mu^2 A\beta_0}(\beta_0 - 1)^2, \tag{III.76}$$

and t^* represents the time required for the ratio of the number of free ink particles to the total number of ink particles in $\mathcal{V}_f$ to fall to a specified level $\gamma_*, \gamma_\infty < \gamma_* < \dfrac{n_p^f(0)}{n_p}$, i.e.,

$$t^* = \frac{1}{2\mu A} ln \left[\frac{1}{\beta_0} \left\{ \frac{\frac{1}{\mu}\left(\gamma_* + \frac{|B|}{2A}\right) + 1}{\frac{1}{\mu}\left(\gamma_* + \frac{|B|}{2A}\right) - 1} \right\} \right] \tag{III.77}$$

Finally, $\hat{\gamma}$ is the level to which the ratio n_p^f/n_p falls in a given time $\hat{t}$.

Insert Fig. 11

v) Characterizing the Efficiency of the Flotation Deinking Process

By referring to the graph of $\gamma(t)$, we note various quantities which can be used to characterize the effectiveness of the flotation deinking process as it applies to the removal of ink particles in the volume element $\mathcal{V}_f$. First of all, since the greatest slope on the graph of $\gamma(t)$ occurs at $t = 0$, we could characterize the effectiveness of the process by looking at

$$\mathcal{F}_e^0 = |\dot{\gamma}(0)|/\gamma(0) \tag{III.78}$$

Although $\mathcal{F}_e^0$ will not usually be a number between zero and one (so that it does not represent an 'efficiency' in the usual sense), it may still be of considerable interest to know under what set of conditions one can maximize the initial (relative) rate of decrease of the number of free ink particles in $\mathcal{V}_f$. From (III.74),

$$|\dot{\gamma}(0)| = \frac{4\mu^2 A\beta_0}{(\beta_0 - 1)^2} \tag{III.79}$$

However,

$$(\beta_0 - 1)^2 = 4\mu^2/(|y_0| - \mu)^2$$

and, therefore,

$$|\dot{\gamma}(0)| = A(|y_0|^2 - \mu^2) \tag{III.80}$$

If we write $|y_0|$ in the form

$$|y_0| = \frac{|B|}{2A} + \gamma(0)$$

then

$$|y_0|^2 - \mu^2 = \gamma^2(0) + \frac{|B|}{A}\gamma(0) - \frac{C}{A} \tag{III.81}$$

so that

$$|\dot{\gamma}(0)| = A\gamma^2(0) + |B|\gamma(0) - C \tag{III.82}$$

Substituting for A, B, and C from (III.35) and using the definition (III.78), we find that

$$\mathcal{F}_e^0 = n_p k_1 \gamma(0) + \{(n_B - n_p)k_1 + k_2\} - (k_2/\gamma(0)) \tag{III.83}$$

which shows that for fixed values of n_p, n_B, k_1, and k_2, $\mathcal{F}_e^0$ is a function of the initial ratio $n_p^f(0)/n_p$, i.e., of $n_p^f(0)$ alone. If we set $x = n_p^f(0)$, then

$$\mathcal{F}_e^0(x) = k_1 n_p x + [(n_B - n_p)k_1 + k_2] - \frac{k_2}{x}\,, \tag{III.84}$$

so that $\mathcal{F}_e^{0'}(x) = k_1 n_p + k_2/x^2 > 0$; thus, the relative initial ratio $|\dot{\gamma}(0)|/\gamma(0)$ is strictly increasing as the number of initially free ink particles in $\mathcal{V}_f$ increases (for fixed values of n_p, n_B, k_1, and k_2). A more interesting exercise would consist of fixing n_p, n_B, and $n_p^f(0)$ and studying how the expression for $\mathcal{F}_e^0$ varies as one perturbs one or more of the basic physical and/or geometrical parameters which enter into the structure of the kinetic constants k_1, k_2, e.g., one could fix in the individual probabilities that govern the microprocesses, all parameters such as R_p, R_B, v_B, σ, etc., and vary only the measure ϵ of the turbulent flow field in the flotation cell, so as to obtain $\mathcal{F}_e^0 = \mathcal{F}_e^0(\epsilon)$; such exercises will be relegated to a future paper.

Aside from the ratio $\mathcal{F}_e^0$, as given in (III.78), at least three other possible measures of the effectiveness of the flotation process present themselves. A primary goal of the flotation process, localized to the volume element $\mathcal{V}_f$, is to drive the relative number of free particles in $\mathcal{V}_f$ as low as possible; thus, one measure of the efficiency of the process would be the ratio

$$\mathcal{F}_e^\infty = 1 - \frac{\gamma_\infty}{\gamma(0)} \equiv 1 - \frac{n_{p,\infty}^f}{n_p^f(0)} \tag{III.85}$$

By virtue of (III.69), and the definition of $\gamma(0)$,

$$\mathcal{F}_e^\infty \simeq 1 - \left(\frac{n_p}{n_p^f(0)}\right) \frac{k_2}{k_2 + (n_B - n_p)k_1} \tag{III.86}$$

It is an immediate consequence of (III.86), and the fact that $n_{p,\infty}^f < n_p^f(0)$, that for any initial number $n_p^f(0)$ of particles in the volume element $\mathcal{V}_f$, we have $0 < \mathcal{F}_e^\infty < 1$, with $\mathcal{F}_e^\infty \to 1$ as $k_2 \to 0$. Obviously, it is possible to also express $\mathcal{F}_e^\infty$ in (III.86) in terms of the basic geometrical and physical parameters of the flotation deinking system, such as R_p, R_B, σ, v_B, h_{crit}, etc., and to study the variation of $\mathcal{F}_e^\infty$ with respect to variations in one or more of these parameters.

The other two measures of the effectiveness of the flotation deinking model are connected with the definitions of the points (t^*, γ_*) and $(\hat{t}, \hat{\gamma})$ on the graph of $\gamma(t)$ (Fig. 11). Recall that t^*, as given by (III.77), represents the time required for the ratio of the number of free ink particles in $\mathcal{V}_f$ to the total number of particles in $\mathcal{V}_f$ to fall to a specified level $\gamma_*, \gamma_\infty < \gamma_* < \dfrac{n_p^f(0)}{n_p}$. If, for example, one were to specify that $\gamma_* = \dfrac{1}{2}\dfrac{n_p^f(0)}{n_p}$, then (III.77) yields

$$t_{1/2} = \frac{1}{2\mu A} ln \left[\frac{1}{\beta_0} \left\{ \frac{\dfrac{1}{\mu}\left(\dfrac{1}{2}\dfrac{n_p^f(0)}{n_p} + \dfrac{|B|}{2A}\right) + 1}{\dfrac{1}{\mu}\left(\dfrac{1}{2}\dfrac{n_p^f(0)}{n_p} + \dfrac{|B|}{2A}\right) - 1} \right\} \right] \tag{III.87}$$

Again, one could substitute in (III.87) for the rate constants k_1, k_2, in terms of the physical and/or geometrical parameters of the deinking process, and study, e.g., how $t_{1/2}$ depends on the particle radius R_p, the bubble radius R_B, the bubble rising velocity v_B, etc.

Another effectiveness measure which is naturally suggested by the graph of $\gamma(t)$ is connected with the interpretation of the point $(\hat{t}, \hat{\gamma})$ on this graph, i.e., for a given $\hat{t} > 0, \hat{\gamma}$ is the level to which the ratio $n_p(t)/n_p$ falls in time $\hat{t}$, i.e.,

$$\hat{\gamma} = \mu \left[\frac{1 + \beta_0^{-1} e^{-2\mu A \hat{t}}}{1 - \beta_0^{-1} e^{-2\mu A \hat{t}}} \right] - \frac{|B|}{2A} \tag{III.88}$$

Since, for a given time $\hat{t} > 0$, it is desirable to have the ratio $\dfrac{n_p^f(\hat{t})}{n_p} \equiv \hat{\gamma}$ as low as possible, $\hat{\gamma}$ is a reasonable measure of the effectiveness of the flotation deinking process in the localized

region $\mathcal{V}_f$; substituting for k_1 and k_2, again, in terms of the basic geometrical and physical parameters of our model, one can, for fixed $\hat{t}$, n_p, n_B, and $n_p^f(0)$, seek to minimize $\hat{\gamma}$ as a function of one or more of the fundamental parameters; such considerations will be the subject matter of a future paper on the flotation deinking process.

vi) Selected Predictions

Predictions of flotation performance can be obtained by employing the solution (III.48) of the initial value problem (III.40), (III.41) if values for selected physical parameters are chosen (i.e., $R_B, R_p, v_B, \rho_p, \rho_\ell, \epsilon, \sigma, \theta, \phi^*_{crit}, n_B, n_p$, etc.). Before this is done, we note that not all physical parameters are independent of each other, and following Schulze [32], we employ $d_B = (\sigma/\rho_\ell)^{0.6}/\epsilon^{0.4}$ to eliminate surface tension, σ, from the list of required parameters. Additionally, Clift et al. [23] have shown that the terminal bubble rise velocity in pure water is approximately 20-30 cm/s for 1 $mm \leq d_B \leq 20$ mm and is lower for contaminated water systems. Since a flotation cell will typically have surfactants and other contaminants in the system, we assume the bubble rise velocity will be constant over a wide range of bubble diameters and that it will be substantially below that of pure water. Therefore, we assume a constant value of $v_B = 10$ cm/s for these calculations. Liquid properties were also assumed to be constant and correspond to those of water. The remaining system parameters $(R_B, R_p, \rho_p, \epsilon, \theta, \phi^*_{crit}, n_B, n_p)$ were chosen based on experimental and theoretical parametric ranges utilized by other investigators for flotation studies [1, 6, 12-15, 32, 33, 42, 43]. Table 5 summarizes the fixed values, identified as standard conditions, employed in this study and the parametric range if the parameter was varied from its standard value. Finally, we employ the Liepe-Möckel correlation (III.3) for the collision frequency and assume that, at time $t = 0$, all particles were free and unattached to bubbles in the unit volume (i.e.,

$n_p^f(0) = n_p$).

Insert Table 5

Figure 12 displays flotation efficiency as a function of time for selected bubble radii while all other parameters are held at constant standard conditions. For all but the smallest radii ($R_B = 0.1\ mm$), flotation efficiency rises rapidly to a constant value within approximately 2 seconds. This indicates that for a given unit volume, steady-state conditions are quickly reached for the given conditions, and if a stable bubble/particle aggregate is formed within this time, it will remain stable and rise to the flotation cell surface for removal. This figure also indicates that for small bubble radii (on the order of 0.1 mm), flotation efficiency is poor for the given fixed conditions, and as the bubble radius increases, flotation efficiency improves and steady-state conditions are reached in a shorter time period.

Insert Fig. 12

Figures 13 and 14 show flotation efficiency at infinite time (i.e., we employ (III.67) in the definition of flotation efficiency) as a function of bubble radius for selected turbulent energy densities, ϵ, and contact angles, θ, respectively, while all other parameters are at standard conditions. Both figures show that flotation efficiency is poor for small bubble radii, but increases rapidly as the bubble radius increases. Efficiency is also reduced when the turbulent energy density or contact angle is reduced. At small contact angles (Fig. 14), predictions may yield spurious results (efficiencies greater than 1 or less than 0) when the bubble radius is small due to limitations and assumptions incorporated into the model equations. These data were omitted from the figure, which results in efficiency predictions for $\theta = 20°$ and $\theta = 40°$ beginning at $R_B = 0.25\ mm$ and $R_B = 0.15\ mm$, respectively.

Predictions for other flotation performace parameters are ongoing and will be the topic

of a future paper.

Insert Fig. 13

Insert Fig. 14

IV Conclusions.

The macroprocess of flotation deinking has been divided into four basic microprocesses: (1) collision or capture of a particle by an air bubble, (2) adhesion of the particle to an air bubble by sliding, (3) development of a three-phase contact at the air bubble/water/particle interface, and (4) bubble/particle stability or instability after the aggregate has formed. These microprocesses have been described in detail and their associated probabilities of successful completion have been summarized.

A kinetic-or population balance-type model has been developed utilizing two kinetic constants: the first, k_1, governs the overall probability that a free particle will successfully intercept and adhere to an air bubble; the second, k_2, describes the probability that a bubble/particle aggregate will become unstable and separate to yield a "new" free particle in the system. These kinetic constants were presented in terms of the individual microprocess probabilities, which are themselves functions of system parameters such as bubble and particle size and density, fluid viscosity, surface tension, etc.

The solution to the kinetic equation has been presented in terms of the kinetic constants from which a theoretical flotation efficiency has been defined. Additional system performance parameters have also been presented in terms of the kinetic constants, which provide supplemental measures of flotation system performance.

Several modifications to the basic model that have been presented in this paper will

be considered in future work; among these modifications are the following: altering the expression for the collision frequency Z between ink particles and bubbles in the volume element $\mathcal{V}_f$; allowing for a time-dependence relative to the total number of particles and bubbles in the volume element $\mathcal{V}_f$; modifying the assumption that, in $\mathcal{V}_f$, only one ink particle can attach itself to a particular bubble; altering the probability distributions to account for situations in which one has to deal with nonspherical ink particles; changing the basic model from one governed by an ordinary differential equation to a system of such equations; and transitioning from a system governed by ordinary differential equations to one governed by partial differential equations so as to allow for convection/diffusion of both ink particles and bubbles into and out of a typical volume element $\mathcal{V}_f$ in the flotation cell.

Acknowledgement

The work described in this paper was funded by the Member Companies of the Institute of Paper Science and Technology. Their continued support is gratefully acknowledged.

References

1. F.G. Paulsen, R. Pan, D. Bousfield, and E. Thompson, The dynamics of bubble/particle approach and attachment during flotation and the influence of short-range non-hydrodynamic forces on disjoining film rupture, in *2nd Research Forum on Recycling*, pp. 1-12, TAPPI Press, Atlanta, GA, (1993).

2. M.A. McCool, Flotation Deinking, in *Secondary Fiber Recycling,* (Edited by R.J. Spangenberg), pp. 141-162, TAPPI Press, Atlanta, GA, (1993).

3. L.D. Ferguson, Flotation Deinking Technology, in *1995 Deinking Short Course Notes,* Chapter 10, TAPPI Press, Atlanta, GA, (1995).

4. E.T. Woodburn, Mathematical modelling of the flotation process, in *Minerals Sci. Engng.,* **2**, 3-17, (1970).

5. H.J. Schulze, *Physico-chemical Elementary Processes in Flotation,* Elsevier Pub, Amsterdam, (1984).

6. R. Pan, D. Bousfield, and E. Thompson, Modelling particle-bubble dynamics and adhesion in air bubble/solid particle/liquid systems, in *1992 Tappi Pulping Conference Proceedings,* pp. 941-956, TAPPI, Atlanta, GA, (1992).

7. A.M. Gaudin, *Flotation,* 2nd edit., McGraw-Hill, N.Y., (1957).

8. R. Schuhmann, Flotation kinetics I, *J. Phys. Chem.,* **46**, 891-910, (1942).

9. K.L. Sutherland, Kinetics of the flotation process, *J. Phys. Chem.,* **52**, 394-425, (1948).

10. U. Bilsing, Ansätze zur modellierung von flotationsprozessen, *Freiberger Forschungsh,* **A368**, 7, (1981).

11. H. Plate, and H.J. Schulze, Modelling of the overall flotation process based on physico-chemical microprocesses - technique and applications, in *XVII Internat. Mineral Processing Congress*, pp.365-377, Dresden, Sept. 23-28, (1991),

12. R. Pan, F. Paulsen, D. Johnson, D. Bousfield, and E. Thompson, A global model for predicting flotation efficiencies: model results and experimental studies, in *1993 TAPPI Pulping Conference Proceedings*, pp. 1155-1164, TAPPI Press, Atlanta, GA (1993).

13. H.J. Schulze, Flotation as a heterocoagulation process: possibilities of calculating the probability of flotation, in *Coagulation and Flocculation,* (Edited by B. Dobias), pp. 321-353, (1993).

14. H.J. Schulze, The fundamentals of flotation deinking in comparison to mineral flotation, in *1991 TAPPI Recycling Forum Proceedings,* pp. 161-167, TAPPI Pressi, Atlanta, GA (1991).

15. H.J. Schulze, Probability of particle attachment on gas bubbles by sliding, *Advances in Colloid and Interface Science,* **40**, 283-305, (1992).

16. H. Plate, Ph.D. Thesis, ADW, UVR Freiberg/Sa. Chemnitzer Str. 40, unpubl. (work quoted in Schulze [13]).

17. W. Isler, Entstehung und abscheidung von luftblasen in technischen papiersuspension, Thesis No. 6063, ETH Zurich (1978).

18. S.S. Dukhin, N.N. Rulev, and A.S. Dimitrov, *Koagulyastsiya i dinamika tonkikh plenok,* Naukova Dumka, Kiev, (1986).

19. R.H. Yoon, and G.H. Luttrell, The effect of bubble size on fine particle flotation, *Mineral Processing and Extractive Metallurgy Review,* **5**, 101-122, (1989).

20. L.R. Flint, and W.J. Howarth, The collision efficiency of small particles with spherical air bubbles, *Chemical Engineering Sci.,* **26**, 1155-1168, (1971).

21. B.V. Derjaguin, S.S. Dukhin, and N.N. Rulev, *Microflotacija,* Chimija Moskva, (1986).

22. N. Ahmed, and G.J. Jameson, Flotation kinetics, In *Frothing in Flotation,* (Edited by J. Laskowski), pp. 77-99, Gordon and Breach, N.Y., (1989).

23. R. Clift, J.R. Grace, and M.E. Weber, *Bubbles, Drops, and Particles,* Academic Press, N.Y., (1978).

24. A.J. Goldman, R.G. Cox, and H. Brenner, Slow viscous motion of a sphere parallel to a plane wall - I. motion through a quiescent fluid, *Chem. Eng. Sci.,* **22,** 637-651, (1967).

25. S.S. Dukhin, and N.N. Rulev, *Kolloidnyi Zh.,* **48,** 302, (1986).

26. S.L. Goren, The normal force exerted by creeping flow on a small sphere touching a plane, *J. Fluid Mech.,* **41,** 619-625, (1970).

27. B.V. Derjaguin, S.S. Dukhin, and N.N. Rulev, Thin-film capillary hydrodynamic method in the theory of flotation, *Colloid Journal of the USSR,* **39, Part I**, 926-933, (1977).

28. M. Williams, and S. H. Davis, Nonlinear theory of film rupture, *J. Colloid and Interface Science,* **90**, 220-228, (1982).

29. F. Liepe, *Mechan. Verfahrenstechnik, vol. 1*, Verlag Grundstoffindustrie, Leipzig, (1977).

30. W. Albring, *Elementarvorgänge fluider Wirbelbewegungen,* Akademieverlag, Berlin, (1981).

31. A. Scheludko, S.L. Tschaljowska, and A. Fabrikant, Contact between a gas bubble and a solid surface and froth flotation, In *Special Discussions of the Faraday Society: Thin Liquid Films and Boundary Layers,* **1**, 112-117, Academic Press, N.Y., (1970).

32. H.J. Schulze, Hydrodynamik der flotations-elementarvorgänge, *Wochenblatt für Papierfabrikation,* **122**, 160-168, (1994).

33. J.M. Hou, and S.H. Hui, Interfacial phenomena in deinking, in *1993 TAPPI Pulping Conference Proceedings*, pp. 1125-1129, TAPPI Press, Atlanta, GA, (1993), pp. 1125-1129.

34. A. Scheludko, B. Tosev, and B. Bogadiev, Attachment of particles to a liquid surface, *J. Chem Soc. Trans. Faraday,* **72**, 2815-2828, (1976).

35. C. Huh, and L. E. Scriven, Shapes of axisymmetric fluid interfaces of unbounded extent, *J. of Colloid and Interface Science,* **30**, 323-337, (1969).

36. R. Crawford, and J. Ralston, Influence of particle size and contact angle in mineral flotation, *Inst. J. Min. Process,* **23**, pp. 1-24, (1988).

37. F.M. Fowkes, Attractive forces at interfaces, *Industrial and Engineering Chemistry,* **56**, 40-52, (1964).

38. J. Abrahamson, Collision rates of small particles in a vigorously turbulent fluid, *Chem Eng. Sci.,* **30**, 1371-1379, (1975).

39. F. Liepe, and O.H. Möckel, Untersuchungen zum stoffvereinigen in flüssiger phase, *Chem Techn.,* **28,** 205-209, (1976).

40. T.R. Camp, and P.C. Stein, Velocity gradients and internal work in fluid motion, *J. Boston Soc. Civil Engrs.,* **30**, 219-237, (1943).

41. P.G. Saffman, and T.S. Turner, On the collision of drops in turbulent clouds, *J. Fluid Mech.,* **1**, 16-30, (1956).

42. R.A. Stratton, Separation by flotation of contaminants from recycled fiber, in *1992 Contaminant Problems Seminar,* pp. 13-21, Cincinnati, OH, TAPPI Press, (April 28-30, 1992).

43. A. Nguyen-Van, S. Kmet, and H.J. Schulze, Collection events in flotation: The quantitative analysis of the particle-bubble collision and the attachment of particles onto bubble surfaces, in *XIX International Mineral Processing Congress,* San Francisco, CA (October 22-27, 1995).

Appendix: The Thin-Film Equations

In this paper, two forms of the equation which governs the thickness of the thin film separating a particle from a bubble have been introduced, i.e., (II.54), (II.55), which is taken from the work of Derjaguin et al. [27], as reported in Schulze [5], and (II.62), which is taken from the work of Williams and Davis [28]. In this Appendix, we will indicate how (II.54), (II.55), and (II.62) may be viewed as different coordinate realizations of the same coordinate invariant equation

$$\frac{\partial h}{\partial t} = \frac{\sigma}{3\mu_\ell} \bigtriangledown \cdot [h^3 \bigtriangledown \left(\bigtriangledown^2 h \right)] \tag{A1}$$

when one uses the capillary pressure

$$P_\sigma = \sigma \bigtriangledown^2 h \tag{A2}$$

employs the appropriate interpretation of h, and uses mathematical assumptions that correctly reflect the particular nature of the physical problem at hand.

Consider, first of all, (II.62); we claim that this equation is identical with (A1); when the disjoining pressure is just given by the capillary pressure (A2), we employ the polar coordinate system (r, θ) on the bubble surface S_B, which is indicated in Fig. 15a, and we take $x = R_B \theta$, i.e., the arc length on a great circle of the spherical bubble as measured from the north pole. Indeed, in the aforementioned coordinate system, if h is the distance from the particle surface to the bubble surface (as measured along the radial line joining the centers of the particle and the bubble) then

$$\begin{aligned} \bigtriangledown^2 h &= \frac{\partial^2 h}{\partial r^2} + \frac{1}{r}\frac{\partial h}{\partial r} + \frac{1}{r^2}\frac{\partial^2 h}{\partial \theta^2} \\ &\equiv \frac{1}{r^2}\frac{\partial^2 h}{\partial \theta^2} \end{aligned} \tag{A3}$$

as $h = h(\theta)$. However, with $x = R_B\theta$,

$$\begin{cases} \left.\dfrac{\partial h}{\partial \theta}\right|_{S_B} = \dfrac{\partial h}{\partial x}\dfrac{\partial x}{\partial \theta} \equiv R_B \dfrac{\partial h}{\partial x} \\ \left.\dfrac{\partial^2 h}{\partial \theta^2}\right|_{S_B} = \dfrac{\partial}{\partial x}\left(R_B \dfrac{\partial h}{\partial x}\right)\dfrac{\partial x}{\partial \theta} \equiv R_B^2 \dfrac{\partial^2 h}{\partial x^2} \end{cases}$$

so that

$$\left.\nabla^2 h\right|_{S_B} = \left.\frac{1}{R_B^2}\frac{\partial^2 h}{\partial \theta^2}\right|_{S_B} \equiv \frac{\partial^2 h}{\partial x^2} \tag{A4}$$

Thus,

$$P_\sigma|_{S_B} = \sigma \frac{\partial^2 h}{\partial x^2} \tag{A5}$$

Also,

$$\begin{aligned} \left(\nabla|_{S_B}\right) &= \left.\left(\frac{\partial}{\partial r}, \frac{1}{r}\frac{\partial}{\partial \theta}\right)\right|_{r=R_B} \\ &= \left(0, \frac{1}{R_B}\frac{\partial}{\partial \theta}\right) \\ &\equiv \left(0, \frac{\partial}{\partial x}\right) \end{aligned} \tag{A6}$$

so that

$$\begin{aligned} \nabla P_\sigma|_{S_B} &= \left(0, \left.\frac{\partial}{\partial x}P_\sigma\right|_{S_B}\right) \\ &= \left(0, \sigma\frac{\partial^3 h}{\partial x^3}\right) \end{aligned} \tag{A7}$$

Finally

$$\begin{aligned}
\nabla \cdot (h^3 \nabla P_\sigma|_{S_B}) &= \nabla \cdot \left(0, \sigma h^3 \frac{\partial h}{\partial x^3}\right) \\
&= \left(\frac{1}{r}\frac{\partial}{\partial r} r, \frac{1}{r}\frac{\partial}{\partial \theta}\right)\Bigg|_{S_B} \cdot \left(0, \sigma h^3 \frac{\partial^3 h}{\partial x^3}\right) \\
&= \frac{1}{R_B}\frac{\partial}{\partial \theta}\left(\sigma h^3 \frac{\partial^3 h}{\partial x^3}\right) \qquad \text{(A8)} \\
&= \frac{\partial}{\partial x}\left(\sigma h^3 \frac{\partial^3 h}{\partial x^3}\right) \\
&= \sigma \frac{\partial}{\partial x}\left(h^3 \left(\frac{\partial P_\sigma}{\partial x}\right)\Bigg|_{S_b}\right)
\end{aligned}$$

or

$$\nabla \cdot \left(h^3 \nabla P_\sigma\Big|_{S_B}\right) \equiv \frac{\partial}{\partial x}\left(h^3 \left(\frac{\partial P_\sigma}{\partial x}\right)\Bigg|_{S_B}\right) \qquad \text{(A9)}$$

as $\sigma \dfrac{\partial^3 h}{\partial x^3} = \dfrac{\partial}{\partial x} P_\sigma\Big|_{S_B}$, by virtue of (A6) and (A7). From (A9), it follows directly that (II.62) is equivalent to (A1), (A2), in the chosen coordinate system on S_B, with $x = R_B\theta$.

Insert Fig. 15

For the derivation of (II.54), (II.55) from (A1), we use the local cylindrical coordinate system shown in Fig. 15b; in this case it is assumed that the spherical particle is approaching the bubble surface normal to that surface. The coordinate x in (II.54), (II.55) will coincide with the local radial coordinate in Fig. 15b. The total distance between the particle surface and the deformed bubble surface is given by

$$h(x,t) \equiv h(r,t) = h_1(x,t) + \hat{h}(t) + \frac{x^2}{2R_p} \qquad \text{(A10)}$$

where h_1 is the distance between the deformed bubble surface and the (originally) undeformed bubble surface at (x,t); $\hat{h}(t)$ is the distance, at time t, between the particle surface and the

undeformed bubble surface at $x = 0$; and $x^2/2R_p$ is the distance, at radial coordinate value x, between the particle surface and the tangent line to the particle surface through the point on that surface which corresponds to $x = 0$. We have

$$\frac{\partial \hat{h}}{\partial t} = v_p \tag{A11}$$

where v_p is the velocity of approach of the particle to the bubble surface as measured along the radial line joining the centers of the particle and the bubble. On the left-hand side of (A1), therefore,

$$\frac{\partial h}{\partial t} = \frac{\partial h_1}{\partial t} + v_p \simeq v_p \tag{A12}$$

as it is assumed in [27] that $\dfrac{\partial h_1}{\partial t} \simeq 0$. Next, in the coordinate system shown in Fig. 15b, with x representing the local *radial* coordinate,

$$\begin{aligned} \nabla^2 h &= \frac{\partial^2 h}{\partial x} + \frac{1}{x}\frac{\partial h}{\partial x} + \frac{1}{x^2}\frac{\partial^2 h}{\partial \theta^2} \\ &\equiv \frac{1}{x}\frac{\partial}{\partial x}\left(x\frac{\partial h}{\partial x}\right) \end{aligned} \tag{A13}$$

as $\dfrac{\partial h}{\partial \theta} \equiv 0$. Thus, by comparing (A13) with (II.50), we see, indeed, that (A2) holds provided R_p^{-1} is small in comparison with $\dfrac{1}{x}\left|\dfrac{\partial h_1}{\partial x}\right|$ and $\left|\dfrac{\partial^2 h_1}{\partial x_1^2}\right|$; indeed, under those circumstances, by (A10)

$$\begin{cases} \dfrac{\partial^2 h}{\partial x^2} = \dfrac{\partial^2 h_1}{\partial x^2} + \dfrac{1}{R_p} \simeq \dfrac{\partial^2 h_1}{\partial x^2} \\ \dfrac{1}{x}\dfrac{\partial h}{\partial x} = \dfrac{1}{x}\dfrac{\partial h_1}{\partial x} + \dfrac{1}{R_p} \simeq \dfrac{1}{x}\dfrac{\partial h_1}{\partial x} \end{cases} \tag{A14}$$

Thus, to the degree of approximation associated with (A14), (A13) becomes

$$\nabla^2 h \simeq \nabla^2 h_1 = \frac{1}{x}\frac{\partial}{\partial x}\left(x\frac{\partial h_1}{\partial x}\right) \tag{A15}$$

Continuing, we have

$$\begin{aligned}
\nabla(\nabla^2 h) &\simeq \nabla(\nabla^2 h_1) \\
&= \left(\frac{\partial}{\partial x}\nabla^2 h_1, \frac{1}{x}\frac{\partial}{\partial \theta}\nabla^2 h_1\right) \\
&= \left(\frac{\partial}{\partial x}\left\{\frac{1}{x}\frac{\partial}{\partial x}\left(x\frac{\partial h_1}{\partial x}\right)\right\}, 0\right) \\
&= \left(\frac{\partial^3 h_1}{\partial x^3} + \frac{1}{x}\frac{\partial^2 h_1}{\partial x^2} - \frac{1}{x^2}\frac{\partial h_1}{\partial x}, 0\right)
\end{aligned} \tag{A16}$$

and

$$\begin{aligned}
\nabla \cdot [h^3 \nabla (\nabla^2 h)] &\simeq \nabla \cdot [h^3 \nabla (\nabla^2 h_1)] \\
&= \frac{1}{x}\frac{\partial}{\partial x}\left[x h^3 \nabla (\nabla^2 h_1)\right] \\
&= \frac{1}{x}\frac{\partial}{\partial x}\left[x h^3 \left(\frac{\partial^3 h_1}{\partial x^3} + \frac{1}{x}\frac{\partial^2 h_1}{\partial x^2} - \frac{1}{x^2}\frac{\partial h_1}{\partial x}\right)\right]
\end{aligned} \tag{A17}$$

By virtue of (A17) and (A12), therefore, (A1) assumes the form

$$\frac{1}{x}\frac{\partial}{\partial x}\left[x h^3 \left(\frac{\partial^3 h_1}{\partial x^3} + \frac{1}{x}\frac{\partial^2 h_1}{\partial x^2} - \frac{1}{x^2}\frac{\partial h_1}{\partial x}\right)\right] = \left(\frac{3\mu_\ell}{\sigma}\right) v_p \tag{A18}$$

or

$$\frac{\partial}{\partial x}\left[x h^3 \left(\frac{\partial^3 h_1}{\partial x^3} + \frac{1}{x}\frac{\partial^2 h_1}{\partial x^2} - \frac{1}{x^2}\frac{\partial h_1}{\partial x}\right)\right] = \left(\frac{3\mu_\ell v_p}{\sigma}\right) x$$

an integration of which yields

$$x h^3 \left(\frac{\partial^3 h_1}{\partial x^3} + \frac{1}{x}\frac{\partial^2 h_1}{\partial x^2} - \frac{1}{x^2}\frac{\partial h_1}{\partial x}\right) = \left(\frac{3\mu_\ell v_p}{2\sigma}\right) x^2 + C \tag{A19}$$

Setting $x = 0$ in (A19), we see that the constant of integration $C = 0$ so that

$$\frac{\partial^3 h_1}{\partial x^3} + \frac{1}{x}\frac{\partial^2 h_1}{\partial x^2} - \frac{1}{x^2}\frac{\partial h_1}{\partial x} = \left(\frac{3\mu_\ell v_p}{2\sigma}\right)\frac{x}{h^3} \tag{A20}$$

which, by virtue of (A10), is the same as (II.54), (II.55) if, in the expression (A10) for $h(x,t)$, we follow Derjaguin et al. [27] and replace $h_1(x,t) \simeq h_1(x)$ by $h_1(x,t) \simeq h_1(0)$. We note that our derivation of (II.54), (II.55), from (A1), appears to be unique, the original derivation of (II.54), (II.55) in [27] following from an approximate integration of the Navier-Stokes equation for the thin film situation shown in Fig. 15b.

$R_p(\mu\text{m})$	25	75	125	175	350
$v_{ps}(\text{cm}/s)$	0.2	1.7	2.97	4.36	9.63
$R_B(\text{mm})$	0.25	0.5	1.0	1.5	
$v_B(\text{cm}/s)$	5	10	22	30	

TABLE 1: SOME TYPICAL PARTICLE SETTLING VELOCITIES, v_{ps}, AND BUBBLE-RISING VELOCITIES, v_B, IN WATER [13].

Forces	Intermediate flow conditions	
(nN)	$t = 5ms^{(a)}$	$t = 25ms^{(b)}$
F_{gr}	23.4	6.6
F_{ur}	5.1	1.4
F_T	26.6	0.2
F_{ca}	1.1	5.7
F_L	0.8	2.5
$F_{g\phi}$	11.4	25.2
$F_{w\phi}$	53.4	202.2

$R_p = 75\mu$m; $v_{ps} = 1.66cm\ s^{-1}$; $\rho_p = 2.5$g cm^{-3}; $R_B = 0.05$cm; $v_B = 5$cm s^{-1}; $Re_B = 50$; $Re_B^* = 1.33$; $C_B = 1$; $\sigma = 70mN\ m^{-1}$; $\nu_\ell = 0.01$g cm^{-1} s^{-1}; $h_{crit} = 40nm$.

Initial conditions at $t = 0 : \phi_T = 19°$ and $h(0) = 2.81\mu$m.

Particle gravity force in water: $26.0nN(2.6 \cdot 10^{-3}$g cm $s^{-2})$.

(a) $\phi = 25.9°$; $u_r = -0.36$cm s^{-1}; $u_\phi = 1.24$cm s^{-1}; $G = 5.41s^{-1}$; $Re_B = 0.12$; $\Delta h = h_0 - h_{crit} = 714.7nm$; $v_{pr} = -1.9 \cdot 10^{-2}$cm s^{-1}; $v_{p\phi} = 1.54$cm s^{-1}.

(b) $\phi = 75.4°$; $u_r = -0.1cm\ s^{-1}$; $u_\phi = 2.74$cm s^{-1}; $G = 12.08s^{-1}$; $Re_B = 0.27$; $\Delta h = -4.6nm$; $v_{pr} = 6.16 \cdot 10^{-6}$cm s^{-1}; $v_{p\phi} = 3.50cm\ s^{-1}$

TABLE 2: TYPICAL VALUES OF FORCES ON SLIDING PARTICLES AT INTERMEDIATE FLOW CONDITIONS [15].

	$R_p = 100\mu$m		$R_p = 10\mu$m
	Smooth	Rough	Smooth
P_c	0.75	0.75	0.0075
P_{asl}	0.013	0.013	0.05
P_{tpc}	0.99	—	1.0
P_{stab}	0.4	0.4	1.0

$R_B = 0.05$cm; $v_B = 10$cm s^{-1}; $C_B = 1$; rigid sphere

TABLE 3: INDIVIDUAL PROBABILITIES FOR PARTICLE/BUBBLE AGGREGATE FORMATION AND STABILITY [13].

particles $\rho_p = 2.25$ g/cm^3 $d_{p\max} = 1.4$mm at $d_B = 2.36$mm; $= 0.26$mm at $d_B = 0.3$mm					particles $\rho_p = 1.1$ g/cm^3 $d_{p\max} = 2.4$mm at $d_B = 2.36$mm; $= 0.38$mm at $d_B = 0.3$mm				
	$d_p = 20\mu$m		$d_p = 200\mu$m			$d_p = 200\mu$m		$d_p = 200\mu$m	
	$d_B = 2.36$mm	0.3mm	2.36mm	0.3mm		$d_B = 2.36$mm	0.3mm	2.36mm	0.3mm
P_c	0.0011	0.0075	0.0011	0.0075	P_c	0.0011	0.0075	0.0011	0.0075
P_{asl} $C_B = 4$	0.23	0.70	0.15	0.29	P_{asl} $C_B = 4$	0.23	0.71	0.12	0.36
P_{asl} $C_B = 1$	0.20	0.21	0.11	0.086	P_{asl} $C_B = 1$	0.002	0.03	$2.3 \cdot 10^{-4}$	0.003
P_{stab}	1	1	1	0.52	P_{stab}	1	1	1	0.92

$\rho_\ell = 1\text{g/cm}^3; \nu_\ell = 0.01\text{g/cm} \cdot s$ at $\epsilon = 1.3W/\text{kg}; d_B = 2.36\text{mm}; v_B = 10\text{cm}/s;\ Re_B = 236$

$\sigma = 50mN/m; \theta = 60°$

mean bubble size: $d_B = (\sigma/\rho_\ell)^{0.6}/\epsilon^{0.4}$ at $\epsilon = 130W/\text{kg} : d_B = 0.3\text{mm}; v_B = 2\text{cm}/s;\ Re_B = 7.48$

TABLE 4: FURTHER PROBABILITIES FOR PARTICLE/BUBBLE AGGREGATE FORMATION AND STABILITY [32].

Parameter	Minimum Value Used in the Literature	Maximum Value Used in the Literature	Parametric Range Utilized in this Study	Standard Conditions
$R_p(\mu m)$	1	600	1-500	50
$R_B(mm)$	0.15	2	0.1-5.0	0.5
$\rho_p(g/cm^3)$	1	7.5	1.0-3.0	1.3
$\rho_\ell(g/cm^3)$	1	1	-	1
$v_B(cm/s)$	1.25	30	-	10
$\mu_\ell(cP)$	1	1	-	1
$\epsilon(W/kg)$	1	130	1-400	10
$\sigma(dynes/cm)$	35	73	$d_B = (\sigma/\rho_\ell)^{0.6}/\epsilon^{0.4}$	$d_B = (\sigma/\rho_\ell)^{0.6}/\epsilon^{0.4}$
$\theta(degrees)$	5	105	5-120	60
$\phi^*_{crit}(degrees)$	33	72	5-85	60
n_B	-	-	100-10000	1000
n_p	-	-	1-1000	100

TABLE 5: PARAMETRIC RANGES OF THE VARIOUS FLOTATION PARAMETERS ADDRESSED IN THE LITERATURE AND UTILIZED IN THIS STUDY [1, 6, 12-15, 32, 33, 42, 43].

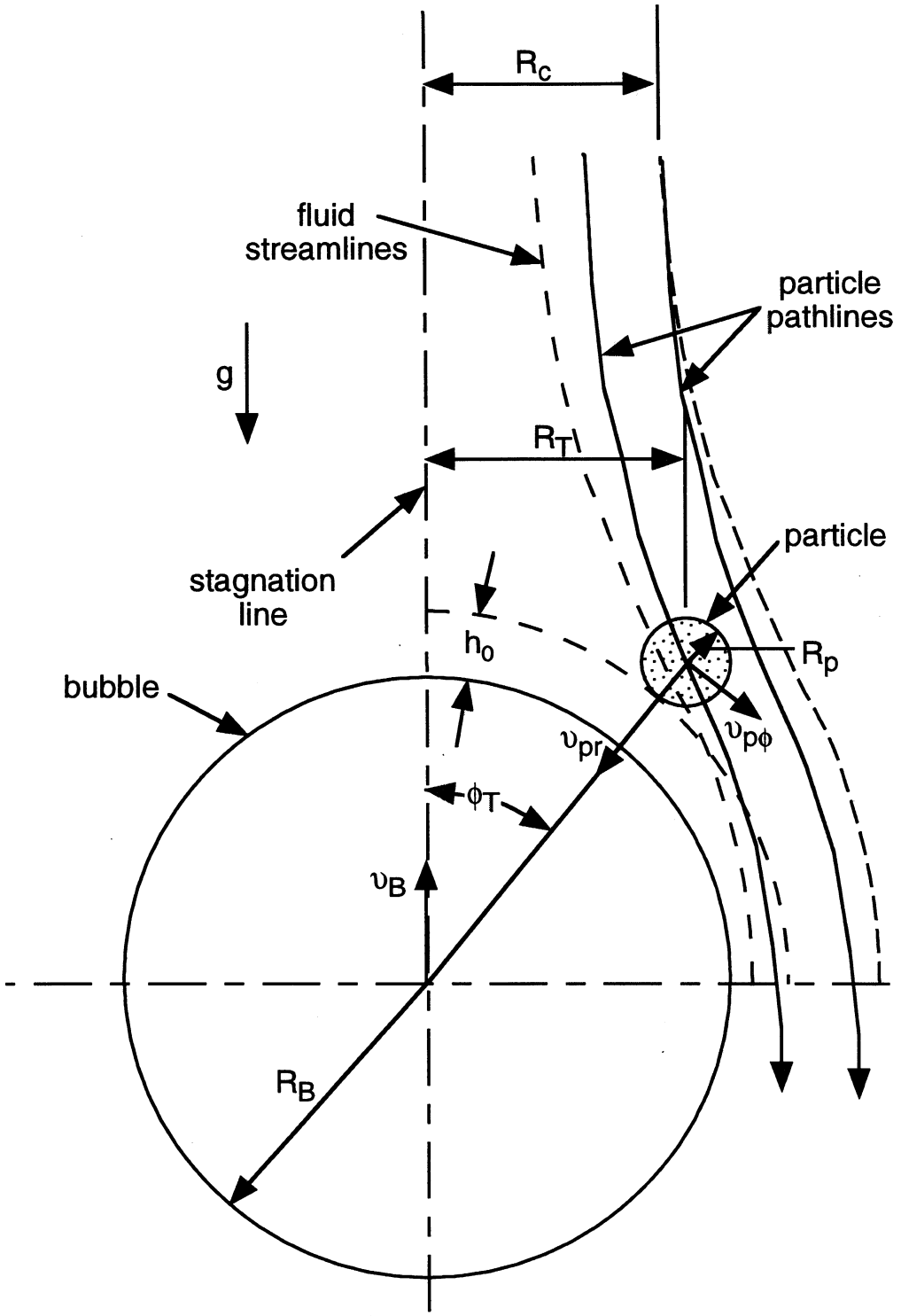

Figure 1: A particle intercepting an air bubble at angle ϕ_T.

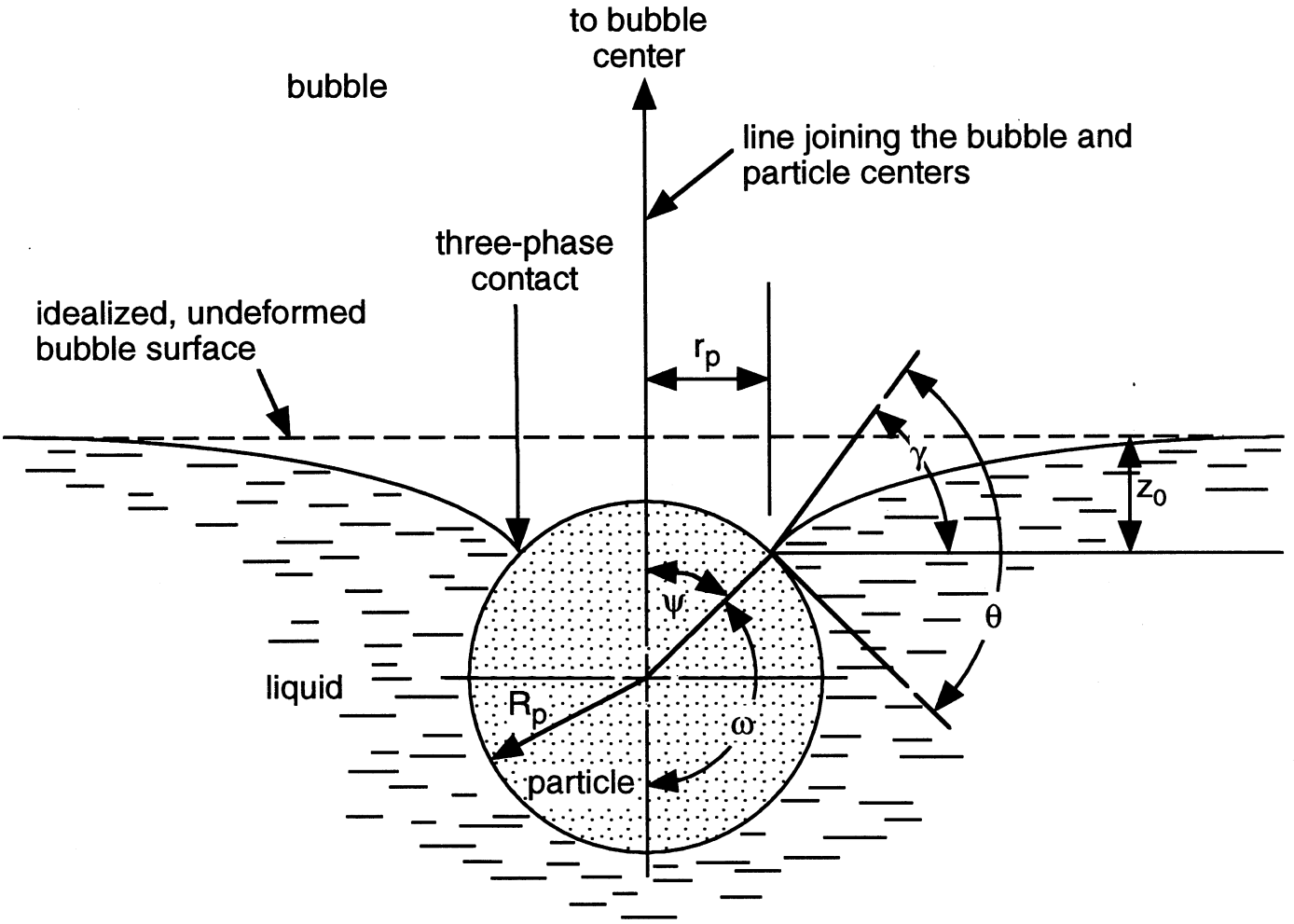

Figure 2. Three-phase contact between the bubble, particle, and fluid regions.

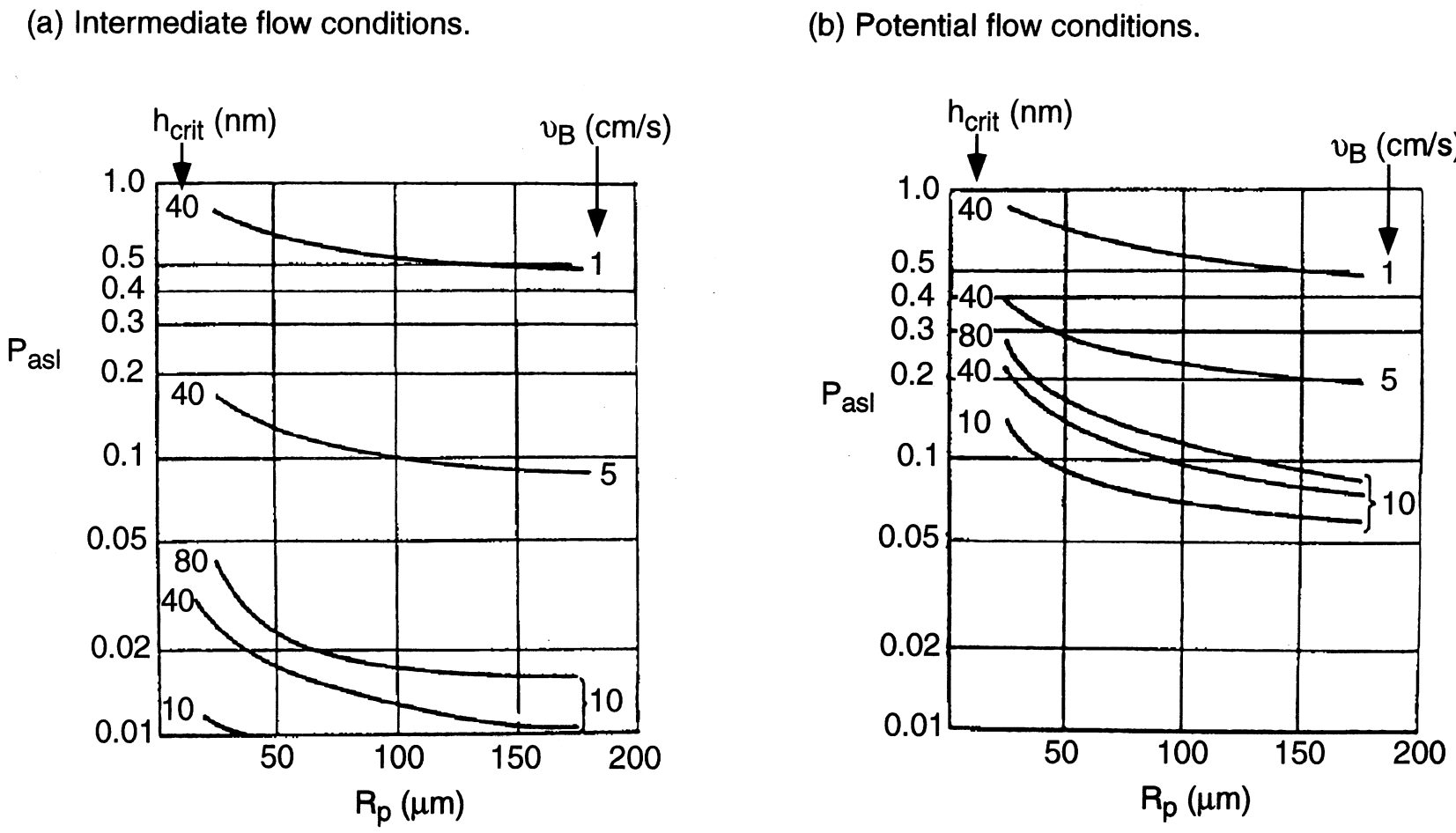

Figure 3: Probability of particle adhesion by sliding, P_{asl}, as a function of R_p, v_B, and h_{crit} for $R_B = 0.5\ mm$, $\sigma = 70\ mN/m$, $\rho_p = 2.5\ g/cm^3$, and $Re_B = 100$. (a) Intermediate flow conditions with $C_B = 1$. (b) Potential flow conditions with $C_B = 4$. (Reprinted with permission from H.T. Schulze, "Flotation as a Heterocoagulation Process: Possibilities of Calculating the Probability of Flotation," in *Coagulation and Flocculation*, B. Dobias (ed), p. 343. Copyright ©1993, M. Dekker.)

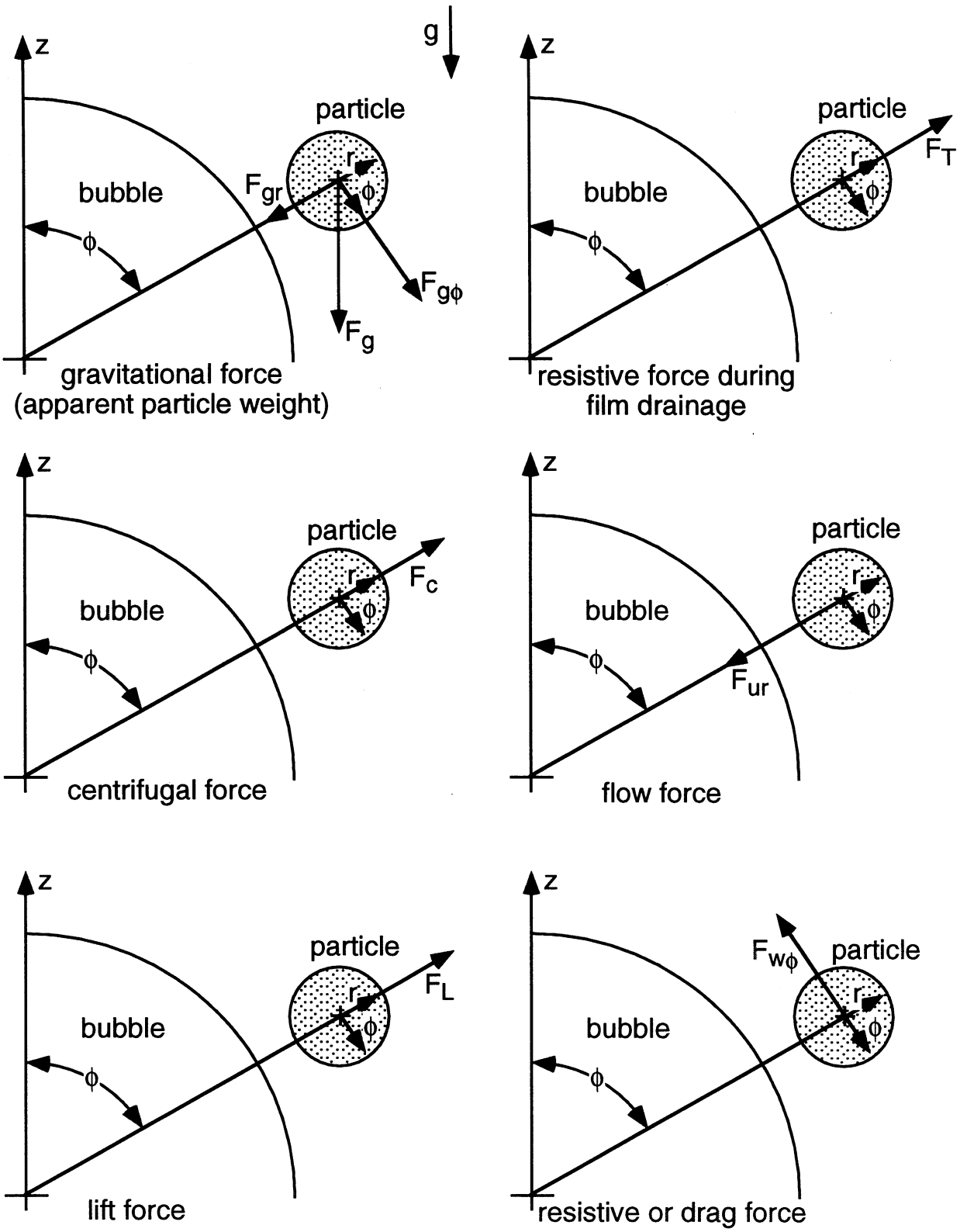

Figure 4: Forces acting on a particle as it slides around a bubble.

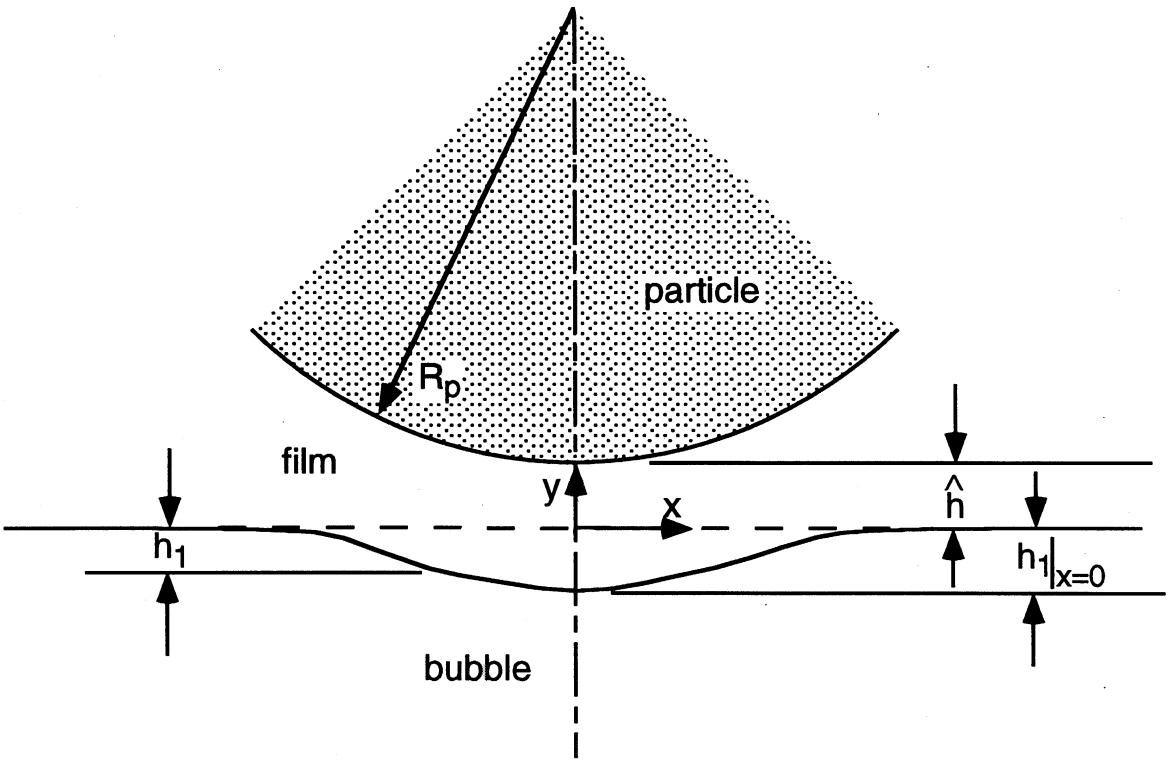

Figure 5: Schematic of the thin film formed between the bubble and particle.

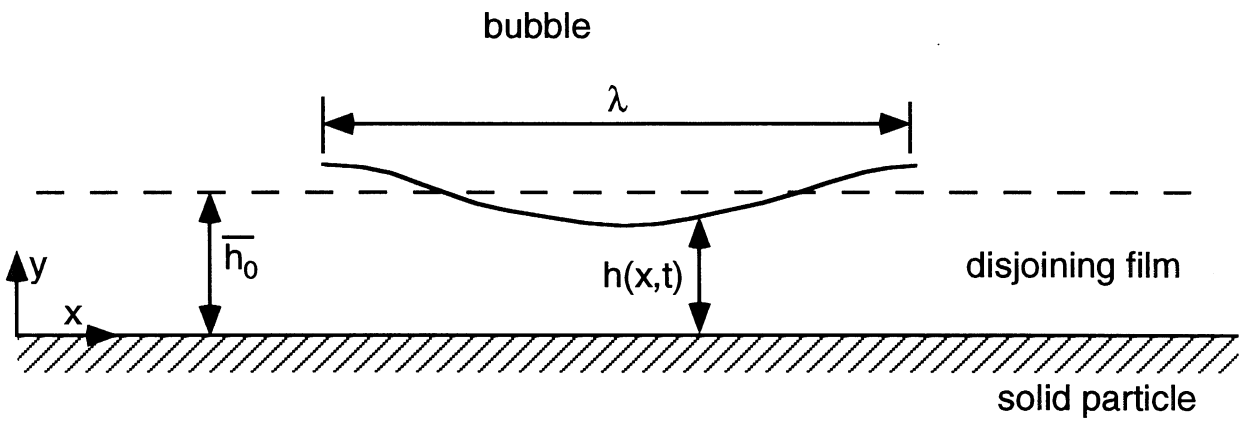

Figure 6: Thin film geometry employed by Paulesen et al. [1].

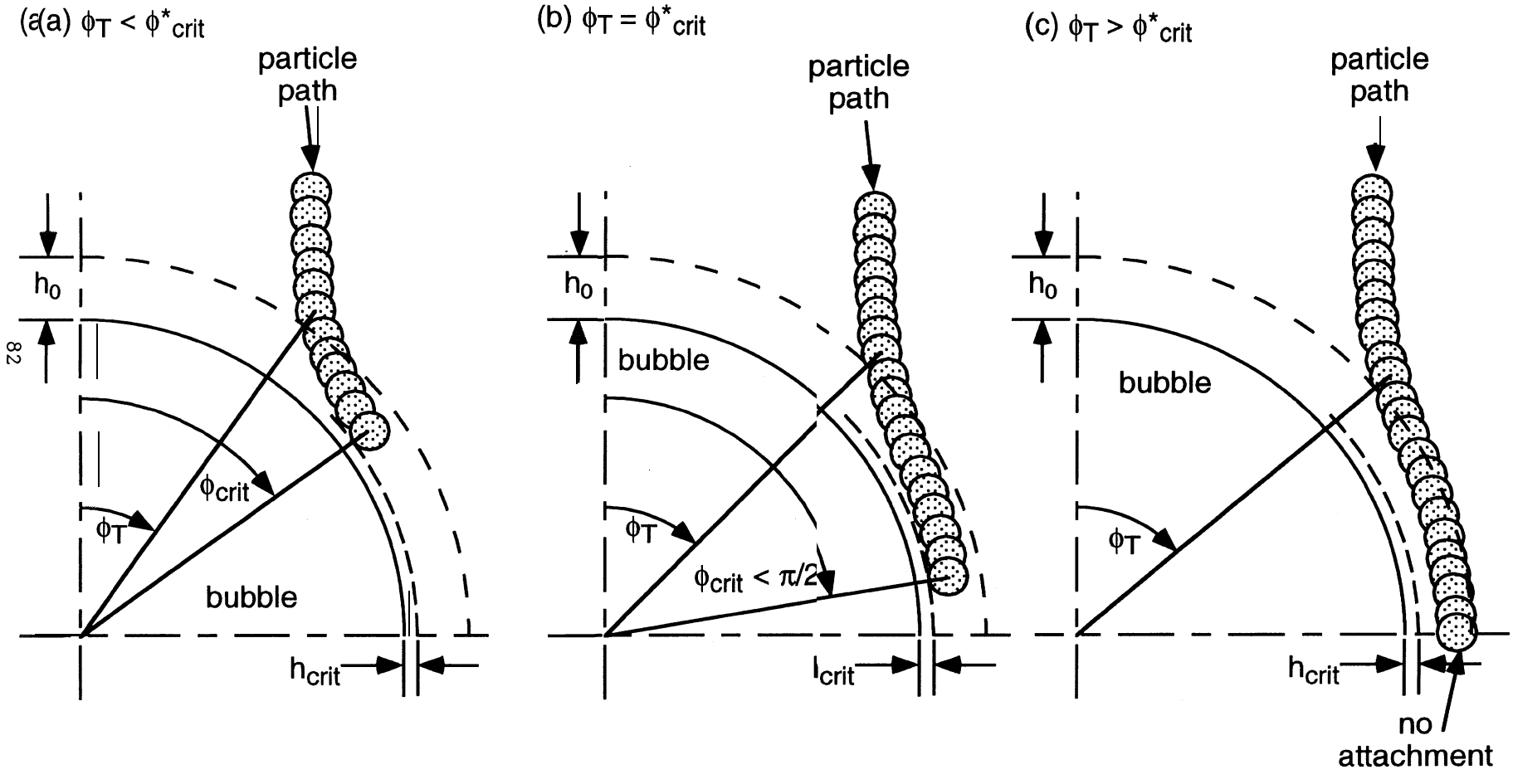

Figure 7: Relationship between the touching angle, ϕ_T, and the critical position angle ϕ^*_{crit}.

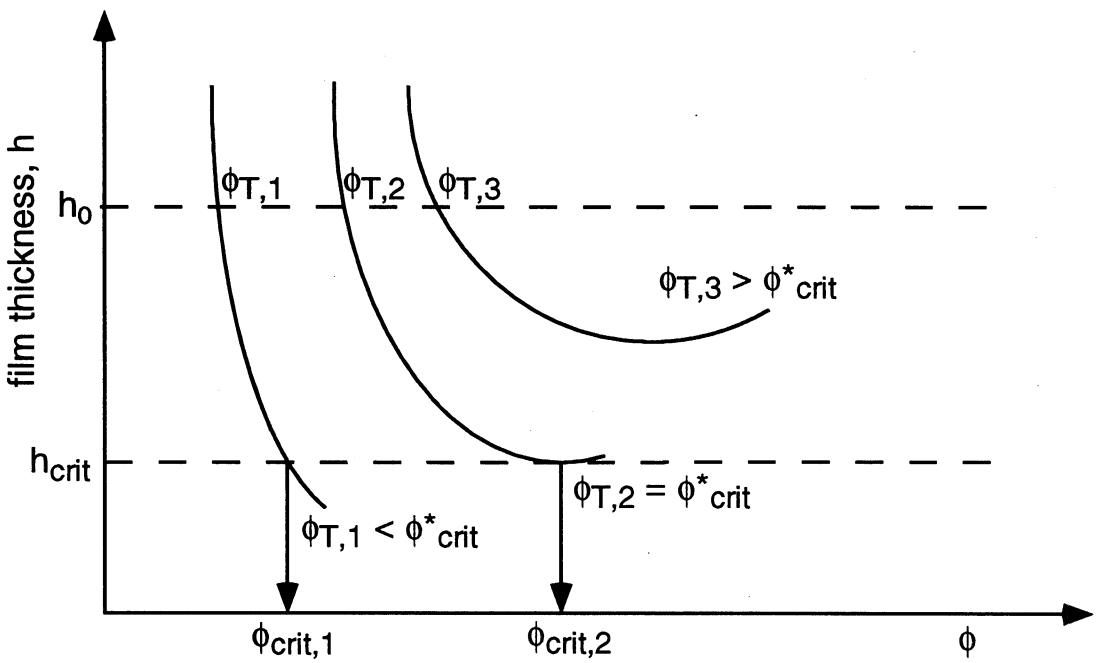

Figure 8: The relationship of ϕ^*_{crit} with respect to ϕ_T and h_{crit}.

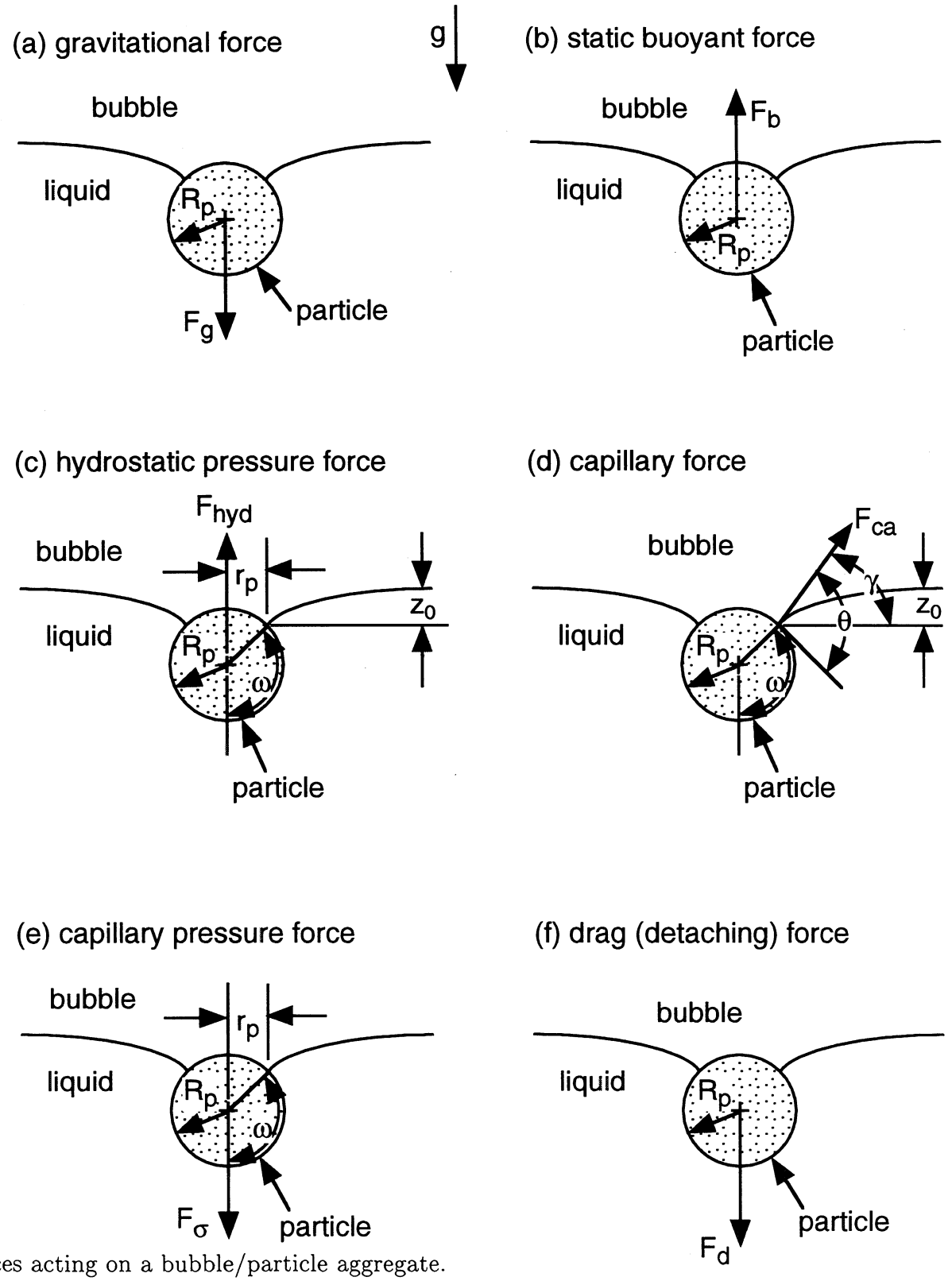

Figure 9: Forces acting on a bubble/particle aggregate.

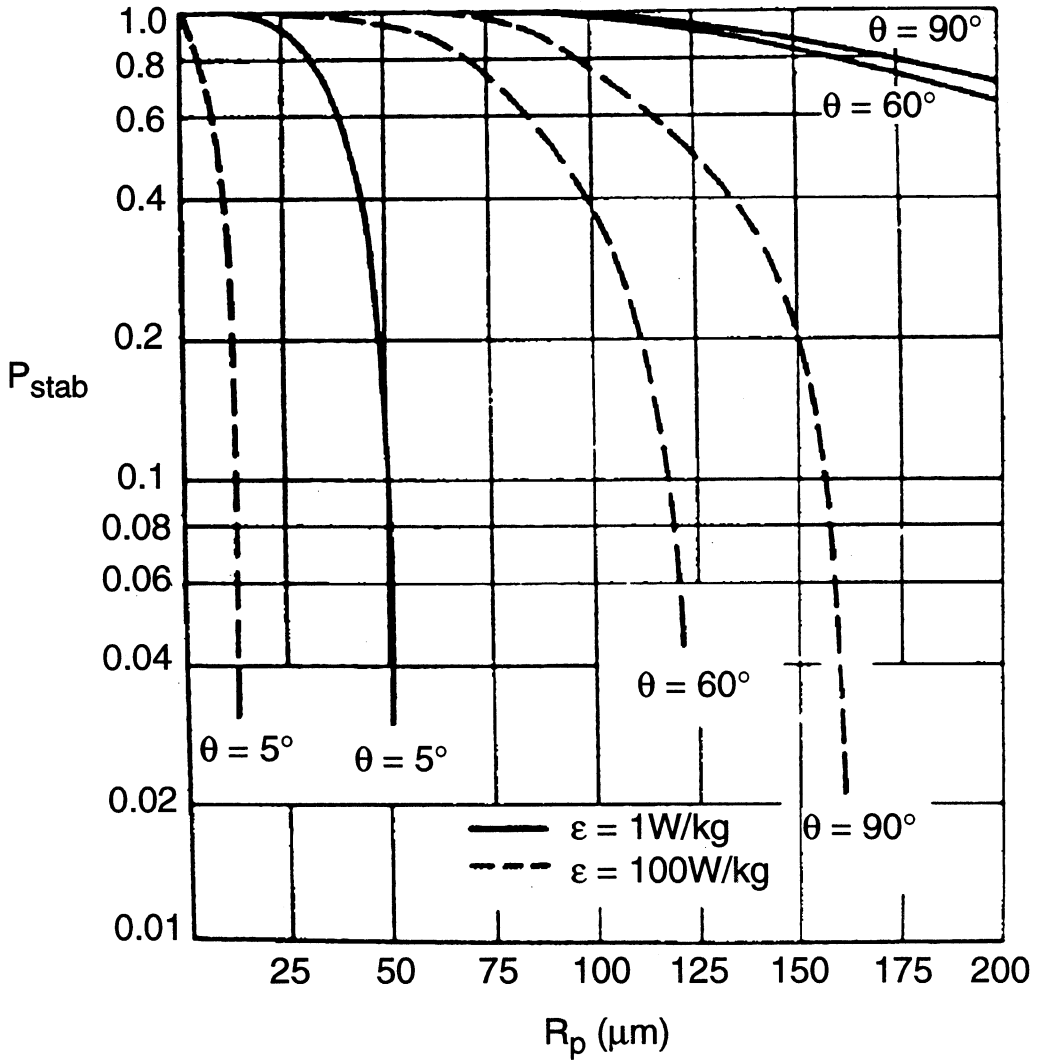

Figure 10: Probability of bubble/particle aggregate stability, P_{stab}, as a function of particle radius, contact angle, and turbulent energy dissipation in a flotation cell for $R_B = 0.5\ mm$, $\sigma = 70\ mN/m$ and $\rho_p = 2.5\ g/cm^3$. (Reprinted with permission from H.T. Schulze, "Flotation as a Heterocoagulation Process: Possibilities of Calculating the Probability of Flotation," in *Coagulation and Flocculation*, B. Dobias (ed), p. 349. Copyright ©1993, M. Dekker.)

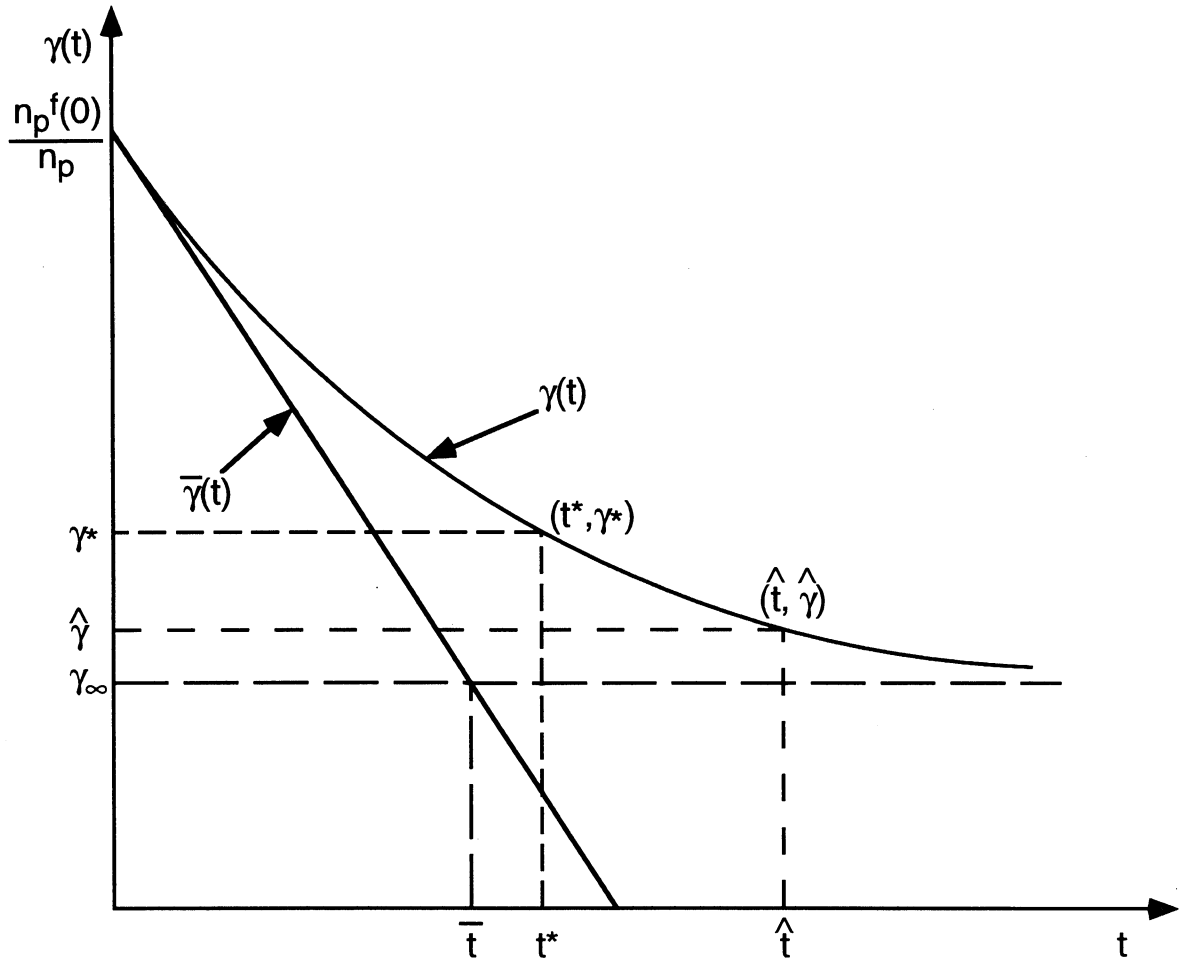

Figure 11: Performance parameters identified with the flotation model.

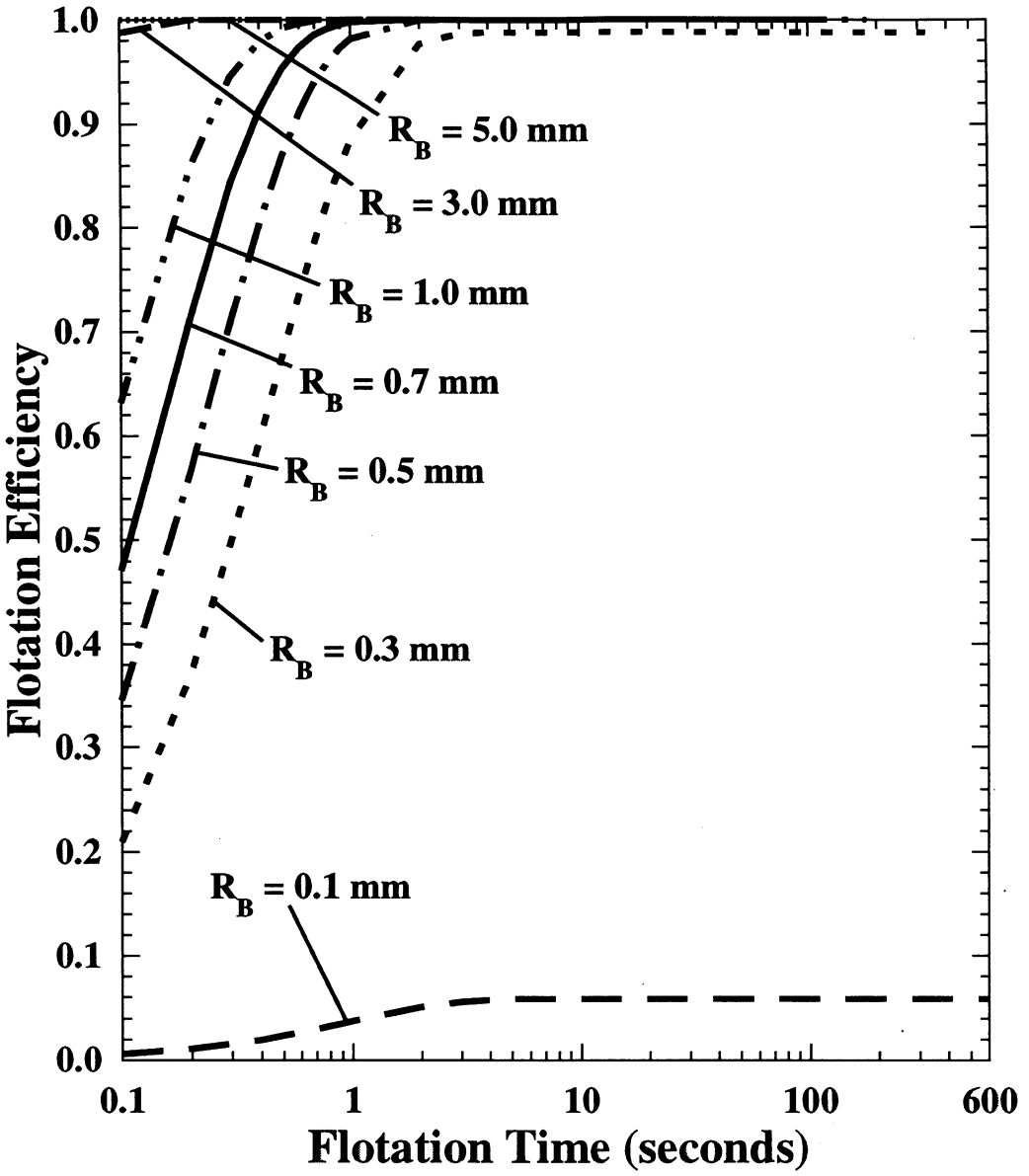

Figure 12: Flotation efficiency as a function of flotation time for selected bubble radii, R_B. All other parameters are at standard conditions: $R_p = 50\ \mu m$, $\rho_p = 1.3\ g/cm^3$, $\epsilon = 10\ W/kg$, $\theta = 60°$, $\phi_{crit} = 60°$, $n_B = 1000$, and $n_p = 100$.

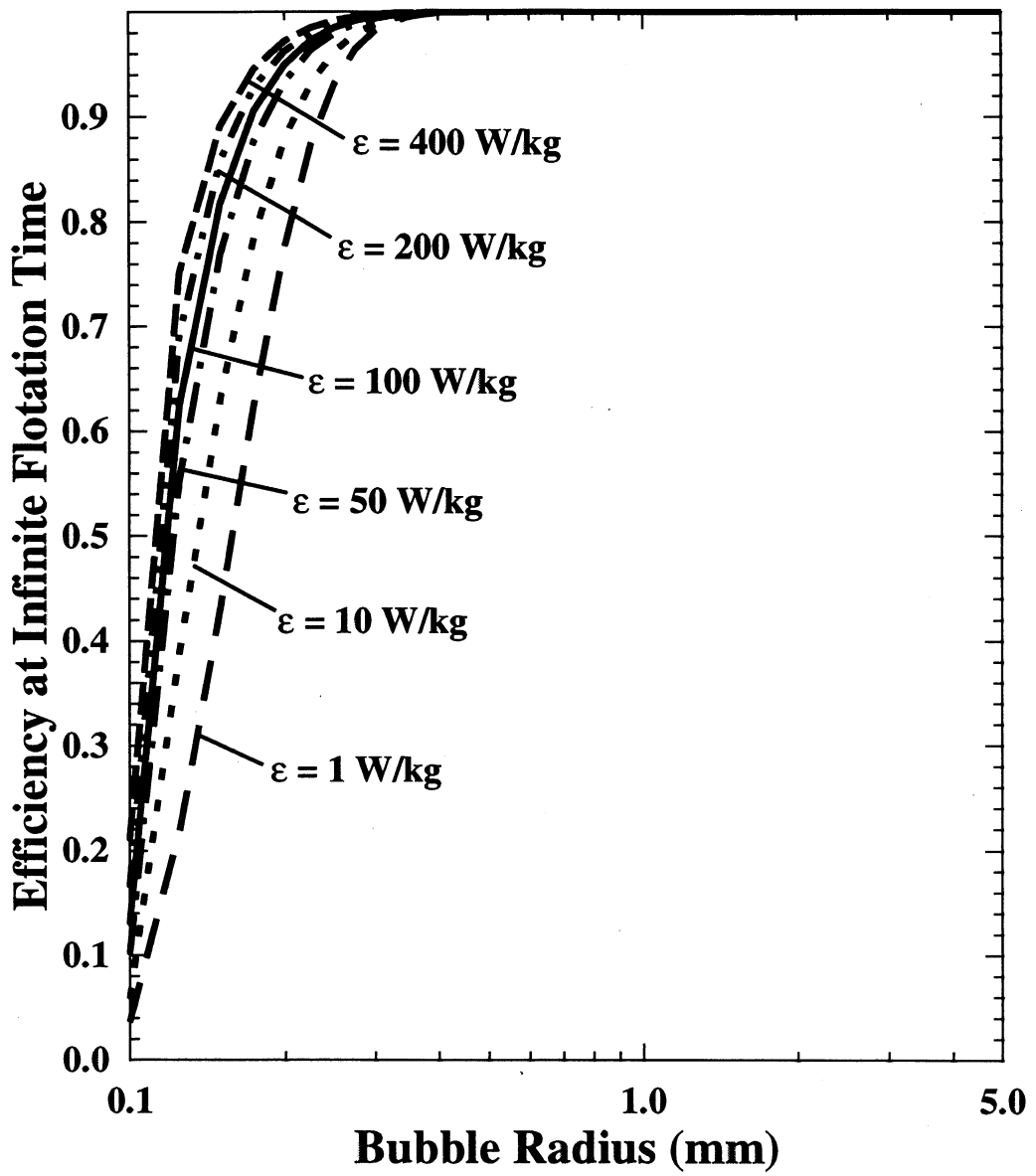

Figure 13: Flotation efficiency at infinite time as a function of bubble radius, R_B, for selected turbulent energy densities, ϵ. All other parameters are at standard conditions: $R_p = 50\ \mu m$, $\rho_p = 1.3\ g/cm^3$, $\theta = 60°$, $\phi^*_{crit} = 60°$, $n_B = 1000$, and $n_p = 100$.

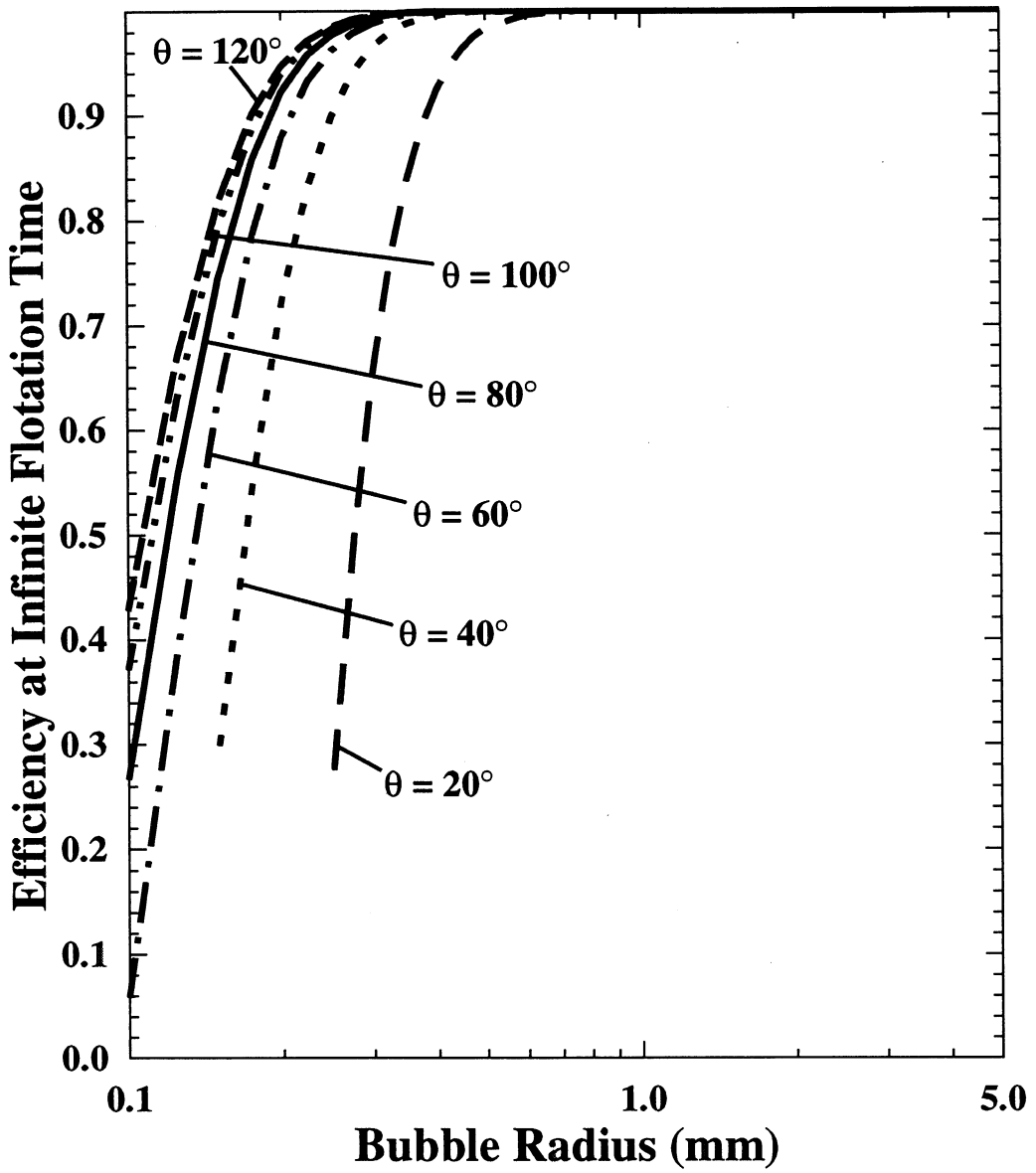

Figure 14: Flotation efficiency at infinite time as a function of bubble radius, R_B, for selected contact angles, θ. All other parameters are at standard conditions: $R_p = 50\ \mu m$, $\rho_p = 1.3\ g/cm^3$, $\epsilon = 10\ W/kg$, $\phi^*_{crit} = 60°$, $n_B = 1000$, and $n_p = 100$.

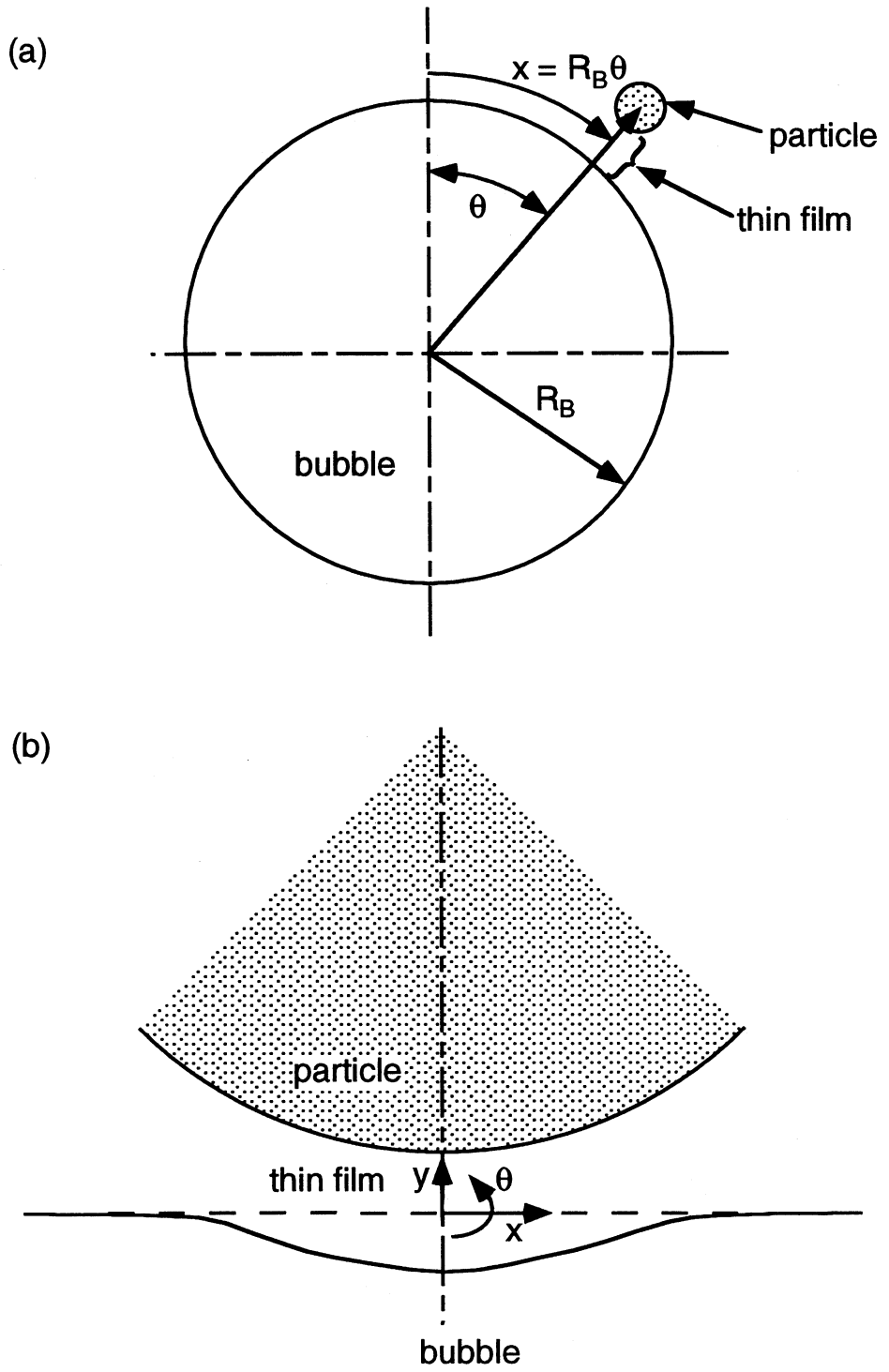

Figure 15: Geometries and coordinate systems associated with the disjoining film dynamics equations.